P-cadherin-induced decorin secretion is required for collagen fiber alignment and directional collective cell migration

Maïlys Le Borgne-Rochet, Lucie Angevin, Elsa Bazellières, Laura Ordas, Franck Comunale, Evgeny Denisov, Lubov Tashireva, Vladimir Perelmuter, Ivan Bièche, Sophie Vacher, et al.

© 2019. Published by The Company of Biologists Ltd | Journal of Cell Science (2019) 132, jcs233189. doi:10.1242/jcs.233189

RESEARCH ARTICLE

P-cadherin-induced decorin secretion is required for collagen fiber alignment and directional collective cell migration

Maïlys Le Borgne-Rochet[1], Lucie Angevin[1], Elsa Bazellières[2], Laura Ordas[1], Franck Comunale[1], Evgeny V. Denisov[3,4], Lubov A. Tashireva[3], Vladimir M. Perelmuter[3], Ivan Bièche[5], Sophie Vacher[5], Cédric Plutoni[6], Martial Seveno[7], Stéphane Bodin[1] and Cécile Gauthier-Rouvière[1,*]

ABSTRACT

Directional collective cell migration (DCCM) is crucial for morphogenesis and cancer metastasis. P-cadherin (also known as CDH3), which is a cell–cell adhesion protein expressed in carcinoma and aggressive sarcoma cells and associated with poor prognosis, is a major DCCM regulator. However, it is unclear how P-cadherin-mediated mechanical coupling between migrating cells influences force transmission to the extracellular matrix (ECM). Here, we found that decorin, a small proteoglycan that binds to and organizes collagen fibers, is specifically expressed and secreted upon P-cadherin, but not E- and R-cadherin (also known as CDH1 and CDH4, respectively) expression. Through cell biological and biophysical approaches, we demonstrated that decorin is required for P-cadherin-mediated DCCM and collagen fiber orientation in the migration direction in 2D and 3D matrices. Moreover, P-cadherin, through decorin-mediated collagen fiber reorientation, promotes the activation of β1 integrin and of the β-Pix (ARHGEF7)/CDC42 axis, which increases traction forces, allowing DCCM. Our results identify a novel P-cadherin-mediated mechanism to promote DCCM through ECM remodeling and ECM-guided cell migration.

KEY WORDS: Collagen fibers, Directional collective cell migration, Traction forces, P-cadherin, Decorin

INTRODUCTION

Directional collective cell migration (DCCM) is characterized by groups of cells that migrate in a coordinated manner, and is a key process during morphogenesis, regeneration and cancer invasion (Friedl and Gilmour, 2009; Friedl et al., 2012; Haeger et al., 2014). DCCM of mesenchymal and epithelial cells is observed during embryo development and also during carcinoma and sarcoma cell invasion (Scarpa and Mayor, 2016; Friedl et al., 2012; Friedl and Gilmour, 2009; Gaggioli et al., 2007). The extracellular matrix (ECM) provides a physical scaffold for cell adhesion and migration by acting on cell tension and by activating signaling pathways through ECM receptors (Egeblad et al., 2010).

During mesenchymal and epithelial DCCM, cadherin-mediated cell–cell adhesion plays an essential role in maintaining cell–cell cohesion and also in allowing mechanosignaling. This is a complex but crucial signaling process elicited at cell–cell contact sites and leading to the generation of traction forces that promote migration. P-cadherin (also known as CDH3), which is overexpressed in epithelial (breast, ovarian, prostate, endometrial, skin, gastric, pancreas and colon) and mesenchymal tumors (rhabdomyosarcomas) with important tumor-promoting effects (van Roy, 2014; Thuault et al., 2013; Vieira and Paredes, 2015), induces DCCM through activation of the β-Pix (also known as ARHGEF7)/CDC42 polarity axis (Halbleib and Nelson, 2006; Plutoni et al., 2016). This polarity regulatory pathway is also involved in DCCM of astrocytes (Cau and Hall, 2005; Osmani et al., 2006) and of anterior visceral endoderm cells in early mouse embryos (Omelchenko et al., 2014). P-cadherin expression predicts the level of intercellular tension in epithelial and mesenchymal cells, and increases intercellular stress anisotropy (Bazellières et al., 2015; Plutoni et al., 2016). This mode of local cell guidance, called plithotaxis, allows the efficient translocation of the entire cell layer, because cells are aligned and migrate along the direction of transmitted stresses. Importantly, this is associated with the development of traction forces that counterbalance the intercellular forces (Maruthamuthu et al., 2011) and drive the cell layer movement. Traction forces are the cell migration engine, and cadherin-based intercellular adhesion stimulates cell–ECM traction forces (Jasaitis et al., 2012; Plutoni et al., 2016; Mertz et al., 2013). However, it is largely unknown how cadherin-mediated mechanical coupling between migrating cells influences force transmission to the ECM. Cadherin mechanosignaling-dependent processes could induce changes in ECM organization that modify ECM–cell interactions in favor of efficient traction force generation. Here, to determine the mechanism of P-cadherin role in DCCM, first we performed a transcriptomic analysis of mesenchymal C2C12 cells that overexpress P-cadherin and the parental line. We found that the matrisome was the main affected group and that *Dcn*, the gene encoding the collagen remodeling molecule decorin, was among the most upregulated genes in mesenchymal C2C12 cells that overexpress P-cadherin compared with the parental line. We then confirmed that P-cadherin expression in C2C12 myoblasts induces decorin expression and secretion, and that decorin is required for P-cadherin-induced DCCM. By performing 2D and 3D migration assays, we found that P-cadherin expression promotes type I collagen fiber alignment in the direction of migration, in a decorin-dependent manner. We then showed that, in breast cancer specimens, collagen fiber alignment is a prominent feature of P-cadherin/decorin-expressing cells at invasion sites. Moreover, decorin is required for P-cadherin-mediated β1 integrin

[1]CRBM, Centre de Recherche en Biologie cellulaire de Montpellier, CNRS UMR 5237, 34000 Montpellier, France Montpellier University, 34000 Montpellier, France. [2]Aix-Marseille University, CNRS, UMR 7288, Developmental Biology Institute of Marseille (IBDM), case 907, 13288 Marseille, Cedex 09, France. [3]Cancer Research Institute, Tomsk National Research Medical Center, 634050 Tomsk, Russia. [4]Tomsk State University, 634050 Tomsk, Russia. [5]Department of Genetics, Institut Curie, 75005 Paris, France. [6]Institute for Research in Immunology and Cancer, Université de Montréal, Montreal, Quebec, Canada. [7]BioCampus Montpellier, CNRS, INSERM, Univ Montpellier, 34094 Montpellier, France.

*Author for correspondence (cecile.gauthier@crbm.cnrs.fr)

E.V.D., 0000-0003-0560-9168; L.A.T., 0000-0003-2061-8417; V.M.P., 0000-0002-7633-9620; I.B., 0000-0002-2430-5429; S.V., 0000-0002-0042-6023; C.P., 0000-0001-6794-301X; C.G-R., 0000-0002-8364-3882

Received 16 April 2019; Accepted 3 October 2019

Journal of Cell Science (2019) 132, jcs233189. doi:10.1242/jcs.233189

and CDC42 activation, via activating threonine dephosphorylation of β-Pix. Finally, through micro-patterned cell monolayers and traction forces microscopy, we demonstrated that decorin is required for P-cadherin-mediated traction force increase and anisotropy.

Our results show that P-cadherin acts a key mediator of DCCM through a new signaling pathway that induces decorin upregulation leading to collagen fiber orientation in the direction of cell migration, and activation of β1 integrin and of the β-Pix/CDC42 axis.

RESULTS

P-cadherin expression is correlated with decorin expression

To identify the underlying molecular mechanisms of P-cadherin-induced DCCM, we compared gene expression, by performing a transcriptome analysis, in C2C12 myoblasts that express P-cadherin (C2C12 Pcad) and control C2C12 cells that express only the LZRS vector (C2C12 LZRS; herein denoted C2C12 CTL). We identified 176 genes that were significantly up- or down-regulated (fold change >3) upon P-cadherin expression (Table S1). Gene ontology (GO) cluster analysis of these genes using PANTHER and GORILLA revealed that P-cadherin expression was associated with a transcriptomic signature of ECM, and particularly of collagen (Fig. 1A; Tables S2 to S5). We also compared the list of genes differentially modified between C2C12 CTL and C2C12 Pcad cell samples to the mouse matrisome signature established in a meta-analysis combining ECM proteomics data from 14 different tissues and tumors (Naba et al., 2016). One third of the modified genes upon P-cadherin expression belonged to the mouse matrisome signature (Fig. 1B). Interestingly, the gene encoding decorin, a collagen-remodeling protein, was one of the five most upregulated genes upon P-cadherin expression (Fig. 1C). We confirmed that decorin mRNA and protein levels were increased in C2C12 Pcad cells compared with C2C12 CTL cells (Fig. 1D,E). Similarly, decorin secretion into the medium was higher in C2C12 Pcad than in C2C12 CTL cells (Fig. 1F), particularly the core protein (38 kDa) that binds to fibrillar collagen (Orgel et al., 2009). This effect was P-cadherin specific because decorin was not upregulated in E-cadherin- (C2C12 Ecad) and R-cadherin-expressing cells (C2C12 Rcad) (Fig. 1D,E). Moreover, P-cadherin-mediated upregulation of decorin required P-cadherin homotypic interaction, because decorin expression was not induced in isolated (non-confluent) C2C12 Pcad cells (Fig. S1A). These results indicate that P-cadherin expression promotes decorin expression and secretion.

Decorin is required for P-cadherin-induced DCCM

Decorin is a class I member of the small leucine-rich proteoglycan family and has a single glycosaminoglycan chain composed of dermatan or chondroitin sulfate with 12 leucine-rich tandem repeats (Iozzo and Schaefer, 2015). Decorin core protein binds to type 1 collagen fibrils (Scott and Orford, 1981; Pogány and Vogel, 1992), and its GAG chain extends laterally from adjacent collagen fibrils to maintain interfibrillar spacing (Scott, 1988; Weber et al., 1996). To understand decorin role in P-cadherin-induced DCCM, we generated stable C2C12 Pcad cell lines that express anti-Dcn shRNA (C2C12 Pcad Dcn shRNA) by retroviral infection. This reduced decorin protein and mRNA expression to the same level as in control C2C12 CTL cells (Fig. 1D,E). By combining time-lapse microscopy, cell tracking and computational analyses, we monitored and quantified cell movements in a 2D migration assay. These experiments showed that after removal of the physical barrier, *Dcn* silencing (C2C12 Pcad Dcn shRNA cells) hindered the P-cadherin-dependent increase in cell velocity and migration persistence observed in C2C12 Pcad cells (Fig. 2A–C; Movie 1). Moreover, analysis of the trajectory angle distribution revealed that decorin expression was needed for P-cadherin-induced directionality increase of individual migrating cells (Fig. 2D). To map cell velocities within entire layers of cells, we used particle image velocimetry analysis (Petitjean et al., 2010). We found that *Dcn* silencing (C2C12 Pcad Dcn shRNA cells) decreased the orientation in the direction of migration of velocity fields and their angle distribution compared with C2C12 Pcad cells (Fig. 2E). As P-cadherin expression increases intercellular stress and plithotaxis within the monolayer during cell migration (Plutoni et al., 2016), we investigated whether decorin contributes to this mechanism. *Dcn* silencing prevented P-cadherin-dependent increase of intercellular stress (Fig. 2F) and plithotaxis (Fig. 2G). Moreover, in C2C12 Pcad *Dcn* shRNA cells that stably expressed human decorin (insensitive to the mouse shRNA; C2C12 Pcad Dcn shRNA Rescue cells), all the examined parameters were similar to those of C2C12 Pcad cells. Decorin protein level reached the level of C2C12 Pcad cells (Fig. 1D), and P-cadherin accumulated at cell–cell contacts in both C2C12 Pcad Dcn shRNA and C2C12 Pcad Dcn shRNA Rescue cells (Fig. S1B). As decorin binds to growth factors (Järvinen and Prince, 2015), we also analyzed cell proliferation and global tyrosine phosphorylation levels in C2C12 CTL, Pcad and Pcad Dcn shRNA cells (Fig. S1C), but did not find any differences.

P-cadherin-induced decorin is needed for cell polarization and focal adhesion orientation

We next analyzed cell organization and cell polarization in the different cell lines. P-cadherin expression induced the formation of a large and oriented protrusion in the direction of migration. The protrusion orientation, but not length was impaired by *Dcn* silencing and was restored in C2C12 Pcad Dcn shRNA Rescue cells (Fig. 3A). Next, we monitored cell polarity by quantifying the position of the centrosome and Golgi relative to the nucleus (Yadav et al., 2009), and found that decorin was required for P-cadherin-induced cell polarization. Indeed, the orientation of the centrosome and Golgi in front of the nucleus toward the protruding edges was perturbed in C2C12 Pcad Dcn shRNA cells, but not in C2C12 Pcad Dcn shRNA Rescue cells (Fig. 3B). Finally, we analyzed focal adhesion (FA) organization by paxillin immunostaining (Zaidel-Bar et al., 2003). The FA orientation in the direction of migration observed in C2C12 Pcad cells was completely abolished by *Dcn* silencing and restored by human decorin expression (Fig. 3C). Analysis of global CDC42 activation using a pulldown assay revealed that P-cadherin-induced CDC42 activation was lost upon *Dcn* silencing (Fig. 3D). Taken together, these results indicate that decorin is required for P-cadherin-mediated CDC42 activation, and orientation of the membrane protrusion, cell organelles and FAs in the migration direction.

Decorin is required for P-cadherin-induced collagen orientation during migration in 2D and 3D matrices

$Dcn^{-/-}$ mice show defects in collagen fibril formation and organization (Danielson et al., 1997), and it has been suggested that decorin could regulate FA reorganization and endothelial cell motility on collagen I (Fiedler et al., 2008). Therefore, we investigated whether P-cadherin-induced decorin expression could affect type I collagen fiber organization.

First, we embedded C2C12 cell spheroids in type I collagen matrix, and monitored 3D cell invasion through the matrix by time-lapse phase-contrast microscopy. After 3 days, C2C12 CTL and C2C12 Pcad cells evaded from the spheroid to colonize the surrounding matrix (Fig. S2A,B). The precise morphological

Journal of Cell Science (2019) 132, jcs233189. doi:10.1242/jcs.233189

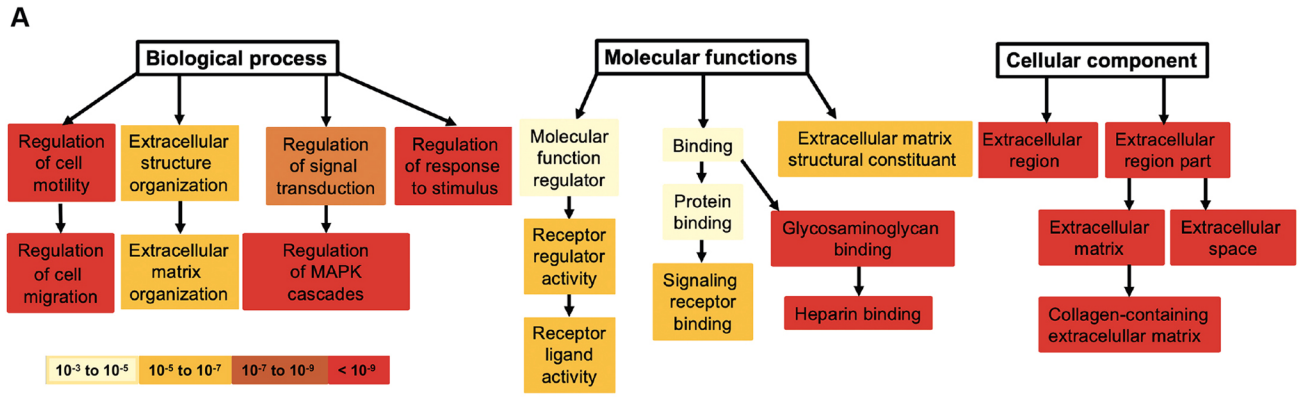

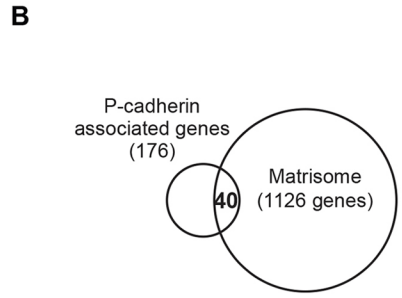

C

Gene title	Gene Symbol	Fold Change CTL vs C2PCad2
guanine deaminase	Gda	25,89854243
semaphorin 3C	Sema3c	13,32339644
nephroblastoma overexpressed gene	Nov	11,70461844
decorin	Dcn	11,3083458
interleukin 1 receptor antagonist	Il1rn	11,20588743

Gene Title	Gene Symbol	Fold Change CTL vs C2PCad9
glutathione S-transferase, alpha 2	Gsta2	20,38200397
guanine deaminase	Gda	20,2925463
vestigial like 2 homolog (Drosophila)	Vgll2	13,43764111
semaphorin 3C	Sema3c	12,77857448
decorin	Dcn	9,937658737

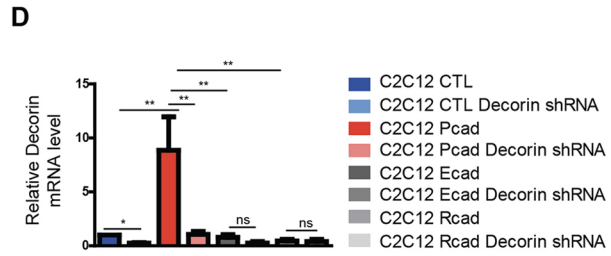

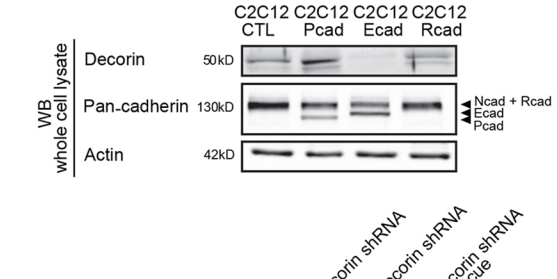

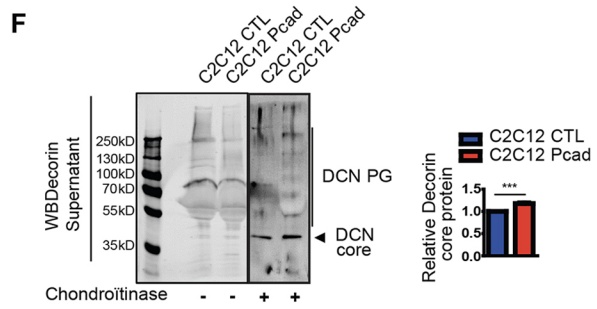

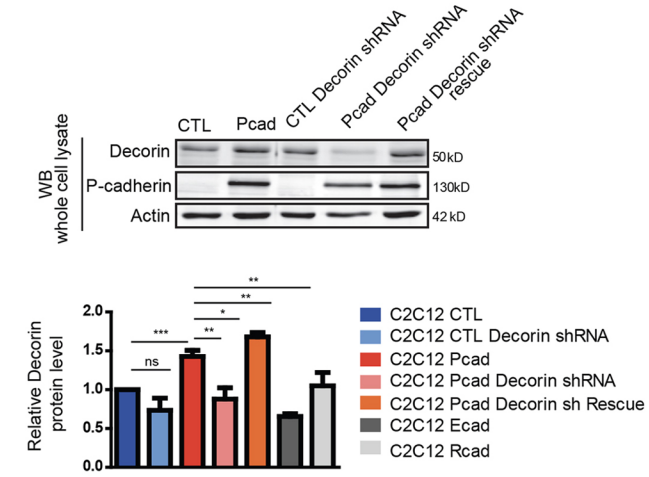

Fig. 1. Decorin expression is promoted by P-cadherin, but not by E- or R-cadherin. (A) The 176 differentially expressed genes identified by transcriptomic analysis in C2C12 Pcad versus to C2C12 CTL were analyzed with GORILLA (Eden et al., 2009). The resulting enriched GO terms are visualized using a DAG representation with color coding reflecting their degree of enrichment. (B) Venn diagrams showing the comparison of the differentially expressed genes identified by transcriptomic analysis in C2C12 Pcad versus C2C12 CTL with the matrisome signature established by Naba et al. (2016). 40 genes of 176 genes of the P-cadherin signature are found in the matrisome signature. (C) The top five upregulated genes upon P-cadherin expression in C2C12 cells. Two clones (#2 and #9, Thuault et al., 2013) as analyzed by transcriptomics. (D) Quantification of decorin mRNA level by RT-qPCR in the indicated cell lines. Cycle threshold (CT) values were normalized to those of mouse *Rpl32*, which encodes the ribosomal protein 32. (E) Representative western blots showing the expression of decorin and the indicated cadherins in chondroitinase-treated whole-cell lysates from the indicated cell lines. The bottom graph shows the quantification of the decorin signal normalized to actin (loading control). (F) Representative western blot of decorin in the supernatant of the indicated cell lines after incubation or not with chondroitinase. The right panel represents the quantification of the decorin core protein signal after chondroitinase treatment (indicated by the arrowhead). The histograms in D–F show the mean±s.e.m. of four independent experiments. **P*<0.05; ***P*<0.01; ****P*<0.001; ns, not significant (two-tailed Mann–Whitney test).

Journal of Cell Science (2019) 132, jcs233189. doi:10.1242/jcs.233189

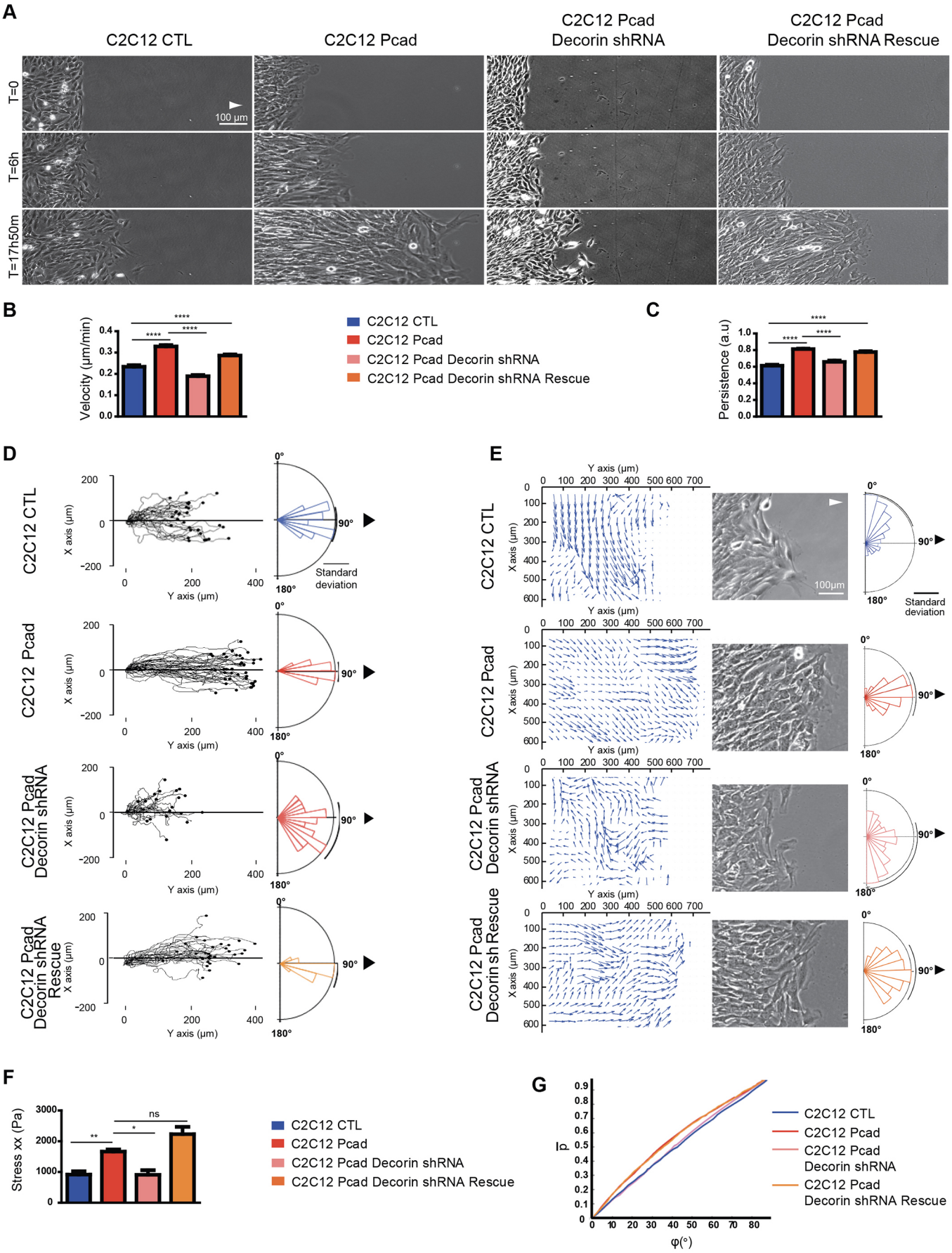

Fig. 2. See next page for legend.

Journal of Cell Science

Journal of Cell Science (2019) 132, jcs233189. doi:10.1242/jcs.233189

Fig. 2. P-cadherin-induced directional collective cell migration is decorin-dependent. (A) Phase-contrast images of 2D cell migration at the indicated time points (0, 6 and 18 h) after barrier removal. (B,C) Velocity (B) and persistence (C) of migration measured between 4 and 24 h after barrier removal. (D) Trajectories during 24 h of 20 representative cells (left) and rose plots showing the mean trajectory angle (right) for the indicated cell lines. The magnitude of each bar represents the fraction of cells with the indicated trajectory angle. Black arrowhead, angle of the direction of migration (90°). The standard deviation is indicated on each rose plot. (E) Velocity fields, corresponding phase-contrast images and rose plots showing the velocity vector orientation as measured using the MatPIV tool in the entire cell layer 10 h after barrier removal. The magnitude of each bar shows the fraction of cells with the indicated angle trajectory. Black arrowhead, angle of the direction of migration (90°). The standard deviation is indicated on each rose plot. (F) Histogram showing the maximum principal intercellular stress parallel to the migration direction (stress xx) measured during 10 h in the indicated cell lines. (G) Cumulative probability distribution of the angle between cellular velocity and maximum principal stress (φ) for the highest quintile of stress anisotropy (as determined by measuring the maximum shear stress, $\overline{p}$) of the different cell lines. All data are the mean±s.e.m. for at least four independent experiments (for tracking, n=111 C2C12 CTL cells, n=133 C2C12 Pcad cells, n=130 C2C12 Pcad Dcn shRNA cells, and n=141 C2C12 Pcad Dcn shRNA Rescue cells). *P<0.05; **P<0.01; ****P<0.0001; ns, not significant (two-tailed Student's t-test). Scale bars: 100 µm.

analysis indicated that C2C12 CTL spheroids migrated as an elongated group of cells that detached one from the other during migration (Fig. S2D, and quantification of the number of cells that detached from the spheroids during the 72 h migration in Fig. S2C). Conversely, C2C12 Pcad cells migrated as a collective group of cells that maintained intercellular contacts and did not detach (Fig. S2C,D). *Dcn* silencing strongly inhibited the invasive potential of C2C12 Pcad cells in the 3D collagen matrix (Fig. S2A,B). This effect was specific to P-cadherin expression because C2C12 Ecad and Rcad cells did not migrate in the 3D collagen matrix.

Then, we analyzed type I collagen fiber organization in the 3D matrix surrounding the cell spheroids using second harmonic generation (SHG) microscopy (Fig. 4A). Cells of the spheroid were revealed by Rhodamine–phalloidin staining. After 72 h, type I collagen fibers assembled as a complex network of fibers that formed intricate meshes. When cells started to invade the 3D collagen matrix, collagen fibers were re-organized in C2C12 CTL cells, and particularly in C2C12 Pcad cells, where cell migration was associated with massive collagen fiber alignment radially from the spheroid in the direction of cell invasion. Quantification of directional collagen fiber orientation, as determined through a Fourier component analysis of directionality on images obtained by second-harmonic generation (SHG) microscopy, showed that P-cadherin, but not E- or R-cadherin, expression promoted collagen fiber orientation towards the direction of migration (Fig. 4B,C). This effect was impaired by *Dcn* silencing.

By using micro-patterned cell monolayers and scanning electron microscopy (SEM), we analyzed collagen fiber organization during 2D migration on type I collagen for 6 h (Fig. 4D). Again, P-cadherin expression was associated with collagen fiber organization and alignment in the migration direction. In control (C2C12 CTL) cells, collagen fibers overlapped and interweaved. Conversely, in C2C12 P-cad cells, collagen fibrils were organized and aligned in the direction of migration. *Dcn* silencing impaired P-cadherin-mediated collagen fiber orientation during migration, while human decorin expression restored collagen fiber orientation in the migration direction. Quantification of directional collagen fiber orientation, through Fourier component analysis of directionality on SEM images, revealed that P-cadherin, but not E- or R-cadherin, expression promoted collagen fiber orientation towards the direction of migration in a decorin-dependent manner (Fig. 4E).

Finally, we assessed whether decorin is expressed in invasive breast tumors in which microdensity increase has been associated with higher collagen density (Skandalis et al., 2011). We did not observe *DCN* mRNA upregulation in a cohort of 527 breast tumor samples, most probably because decorin is expressed both by normal and tumoral cells (Fig. 4F, left panel, the asterisk shows a normal acinus surrounded by tumoral cells). However, low *DCN* mRNA level was significantly associated with a better prognosis in two breast tumor types [triple negative and hormone receptor $(HR)^-$, $ERBB2^+$] (Fig. S3A). The analysis of *CDH3* and *DCN* expression in different morphological structures of breast tumors revealed that their highest levels were found in cells presenting a morphological organization characteristic of invasive tumor cells (Fig. S4D). In human breast tumor samples, decorin protein was expressed by cytokeratin 7 (CK7, also known as KRT7)-positive tumor cells and, to a lower extent, by α-smooth muscle actin (α-SMA)-positive stromal cells (Fig. 4F,G; Table S6). Moreover, immunohistochemistry of serial breast tumor tissue sections allowed identifying migrating tumor cells that co-expressed P-cadherin and decorin and that were surrounded by tracks of aligned collagen fibers (Fig. 4H; Table S6). We also found that specific *CDH3*:*DCN* ratios were associated with poor disease-free survival in patients with HR^+/$ERBB2^-$ and HR^-/$ERBB2^+$ breast tumors (Fig. S3B).

Altogether, these results obtained in 2D and 3D migration assays in type I collagen matrix indicate that P-cadherin expression promotes collagen fiber alignment in the direction of migration and that decorin is required for this process. Moreover, collagen fibers form parallel fascicles that surround P-cadherin and decorin-expressing breast tumor cells in invasive regions.

Decorin is needed for P-cadherin-mediated β1 integrin and CDC42 activation, and for increasing traction force anisotropy and strength

Fibrillar collagen activates the β-Pix/CDC42 axis through β1 integrin (Kutys and Yamada, 2014), and P-cadherin regulates DCCM through β-Pix-mediated CDC42 activation (Plutoni et al., 2016). Therefore, we assessed whether P-cadherin-mediated decorin expression regulates β1 integrin activation during DCCM. To this aim, we plated cells on a 2D collagen matrix because P-cadherin induces collagen fiber alignment through decorin both in 2D and 3D (Fig. 4), and because 2D cell migration along fibers recapitulates migration in a 3D matrix (Doyle et al., 2009). The level of active β1 integrin was high in C2C12 Pcad cells, but not in C2C12 Ecad and Rcad cells, whereas the total β1 integrin level was comparable in all tested cell lines (Fig. 5A; Fig. S5A). Decorin addition, known to increase C2C12 myoblast migration persistence (Goetsch et al., 2011), was associated with an increase of active β1 integrin. Conversely, the level of active β1 integrin was strongly decreased in C2C12 Pcad Dcn shRNA cells, and was restored by human decorin expression (Fig. 5A). We then used the soluble arginine-glycine-aspartic acid (RGD) peptide, which inhibits β1 integrin in our experimental setting (Fig. S5B). We showed that RGD peptide addition affected P-cadherin-induced persistence of migration and cell polarization to the same extent as *Dcn* silencing (Fig. 5B,C; compare with Figs 2A and 3B). Moreover, RGD peptide addition to the collagen type I impaired 3D matrix invasion by C2C12 Pcad cells (Fig. 5D). Nevertheless, in this condition, we still observed collagen reorganization in the areas around the spheroid, but to a lower extent than with C2C12 Pcad migrating cells

Journal of Cell Science (2019) 132, jcs233189. doi:10.1242/jcs.233189

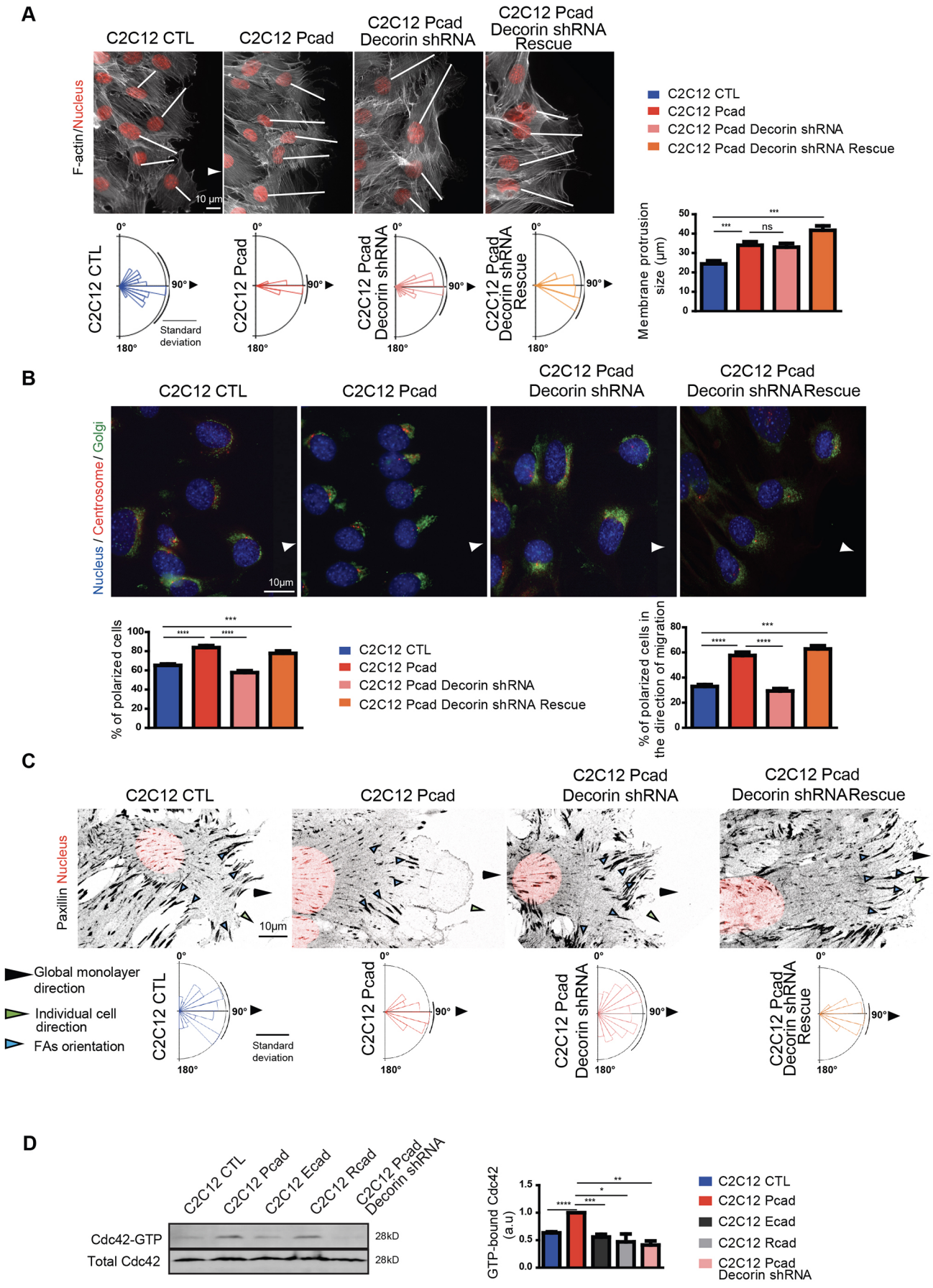

Fig. 3. See next page for legend.

Journal of Cell Science (2019) 132, jcs233189. doi:10.1242/jcs.233189

Fig. 3. Decorin is required for P-cadherin-induced polarization of the front protrusion, of cells and of focal adhesions. (A) Visualization of F-actin (inverted contrast image) and nuclei (red) at the migrating front after 6 h of migration allowed monitoring the front protrusion (white bars). Rose plots showing the front protrusion angle distribution are below each cell line. The magnitude of each bar indicates the front protrusion fraction with the indicated angle. Black arrowhead, angle of the direction of migration (90°). The standard deviation is indicated on each rose plot. The histogram (right) indicates the front protrusion length (n=71 C2C12 CTL cells, n=69 C2C12 Pcad cells, n=80 C2C12 Pcad Dcn shRNA cells, and n=79 C2C12 Pcad Dcn shRNA Rescue cells) from four independent experiments. (B) Migrating cells at the multicellular front (6 h after barrier removal) were stained with Hoechst 33342 (nuclei; blue), anti-pericentrin antibody (centrosomes; red) and Alexa Fluor 488–lectin conjugates (Golgi; green). The histograms show the percentage of migrating cells in which the nucleus, centrosome and Golgi are similarly aligned (i.e. are aligned in the same direction, representing polarized cells) (left panel) and located in the quadrant facing the free space in front of the nucleus, as an indication of cell polarization in the migration direction (right panel) (n=127 C2C12 CTL cells, n=145 C2C12 Pcad cells, n=144 C2C12 Pcad Dcn shRNA cells, and n=152 C2C12 Pcad Dcn shRNA Rescue cells) from four independent experiments. White arrowheads in A and B indicate the direction of migration. (C) Confocal images of the front of migrating cells after staining with an anti-paxillin antibody (FAs) and with Hoechst 33342 (nuclei; red). The rose plots show the angle orientation distribution of FAs calculated using the monolayer migration direction as the reference axis. The area of each bin represents the number of FAs in that direction. Black arrowhead, angle of the direction of migration (90°); green and blue arrowheads show the FA orientations and migration direction of the cell, respectively. The standard deviation is indicated on each rose plot. FAs were analyzed from three independent experiments in n=53 C2C12 CTL cells, n=45 C2C12 Pcad cells, n=43 C2C12 Pcad Dcn shRNA cells, and n=49 C2C12 Pcad Dcn shRNA Rescue cells. (D) The level of GTP-bound CDC42 was evaluated in lysates from the indicated cell lines 6 h after wounding. GTP-bound CDC42 was detected by immunoblotting and quantified (histogram on the right) after normalization to total CDC42. All panels show the mean±s.e.m. $^{**}P$<0.01; $^{***}P$<0.001; $^{****}P$<0.0001; ns, not significant [two-tailed Mann–Whitney test, P-values (D), two-tailed Student's t-test (A,B)]. Scale bars: 10 µm.

(Fig. 5E). This indicates that efficient collagen fiber reorganization requires both decorin secretion and integrin-mediated adhesion. We then asked whether P-cadherin-mediated decorin expression was involved in the activation of the β1 integrin/β-Pix/CDC42 signaling axis. Incubation of C2C12 Pcad cells with the RGD peptide decreased CDC42 activation, indicating that integrins are activated downstream of P-cadherin to allow CDC42 activation (Fig. 5F). As β-Pix must be dephosphorylated at threonine 526 to induce CDC42 activation (Kutys and Yamada, 2014), we monitored β-Pix threonine phosphorylation during migration after DCCM in C2C12 Pcad cells, control C2C12 CTL and C2C12 Pcad Dcn shRNA cells. P-cadherin expression was associated with lower β-Pix threonine phosphorylation (Fig. 5G) and concomitant increase of CDC42 activity (Fig. 3D). Conversely, in C2C12 Pcad Dcn shRNA cells, the β-Pix threonine phosphorylation level was comparable to that of control C2C12 CTL cells (Fig. 5G), while CDC42 activation was markedly reduced (Fig. 3D).

Finally, using micro-patterned cell monolayers and traction-force microscopy, we investigated whether decorin participates in P-cadherin-mediated traction force strength and polarization exerted by the cells on the underlying substrate that drive the cell layer movement. We measured the traction forces parallel (Tx, Movie 2) and perpendicular (Ty) to the direction of migration and calculated the Tx:Ty ratio. As previously shown (Plutoni et al., 2016), P-cadherin expression increased the Tx:Ty ratio. The Tx:Ty ratio was reduced in C2C12 Pcad Dcn shRNA cells (Fig. 5H) and restored in C2C12 Pcad Dcn shRNA Rescue cells. Analysis of the traction force orientation from 0 to 40 µm and from 60 to 140 µm from the leading multicellular row toward the center of the cell layer showed that P-cadherin-induced traction force orientation towards the direction of migration was impaired in C2C12 Pcad Dcn shRNA cells (Fig. 5I; Fig. S5C) and restored in C2C12 Pcad Dcn shRNA Rescue cells.

Taken together, these data demonstrate that P-cadherin-mediated decorin expression specifically activates β1 integrin and decreases β-Pix threonine phosphorylation. This promotes CDC42 activation, leading to an increase in traction force strength and anisotropy towards the migration direction, which are processes required for DCCM.

DISCUSSION

In this study, we identified an original mechanism through which cadherin-mediated mechanical coupling between migrating cells results in force transmission to the ECM to promote cell migration. P-cadherin, a major DCCM inducer, increases the traction force anisotropy and strength that pull the cell layer (Bazellières et al., 2015; Ng et al., 2012; Plutoni et al., 2016). We demonstrated that P-cadherin, but not E- or R-cadherin expression, is associated with collagen fiber organization and alignment in the migration direction and identified decorin, a secreted proteoglycan, as a key player in this process. Collagen fiber alignment facilitates cancer cell invasion by providing tracks on which cells migrate and has a bad prognostic value (Conklin et al., 2011; Drifka et al., 2016; Gjorevski et al., 2015; Levental et al., 2009; Lyons et al., 2011; Provenzano et al., 2008; Riching et al., 2014). Conversely, inhibition of collagen fibril alignment, without affecting ECM composition, blocks tumor cell invasion (Grossman et al., 2016). Here, we experimentally showed that P-cadherin expression specifically promotes collagen fiber alignment concomitantly with polarization of the front protrusion and of FAs in the migration direction and with β1 integrin activation. This is consistent with the observation that FAs are localized along collagen fibers (Wolf et al., 2007). The reorganization of the collagen ECM leads to local stiffening, which enhances integrin-dependent mechanotransduction. Using a mathematical model that takes into account matrix ligand density, stiffness and alignment, it was previously proposed that the increased migration persistence is due to ligand presentation along an axis allowing cells to form and stabilize FAs in a given direction, leading to more efficient migration (Riching et al., 2014). A recent report showed that cadherin-11-mediated cell–cell adhesion regulates the synthesis of ECM proteins, such as collagen and elastin (Row et al., 2016). Our identification of an ECM signature associated with P-cadherin expression also supports the hypothesis that cadherin-mediated adhesion could regulate both ECM production and organization.

We also showed that P-cadherin-induced collagen fiber alignment is mediated by decorin, a secreted proteoglycan that binds to type I collagen fibers and promotes and regulates collagen fibril formation and stability (Chen and Birk, 2013; Kalamajski and Oldberg, 2010; Neame et al., 2000). *Dcn* knock-out in mice leads to perturbed collagen fiber morphology and skin fragility (Danielson et al., 1997). Decorin is known to be involved in several cellular functions, such as morphological changes, cell migration, cell signaling and autophagy (Gubbiotti et al., 2015, 2016; Tufvesson, 2003; Goetsch et al., 2011). Decorin is detected in the tumor microenvironment and can either suppress tumor growth (Bozoky et al., 2014; Csordás et al., 2000; Santra et al., 2000) or promote tumor invasiveness, metastasis and angiogenesis (Dil and Banerjee, 2012, 2011; Banerjee et al., 2003; El Behi et al., 2013; Cawthorn et al., 2012). In two breast tumor types (triple negative and HR^{-}/$ERBB2^{+}$), we found that low DCN mRNA expression level is

Journal of Cell Science (2019) 132, jcs233189. doi:10.1242/jcs.233189

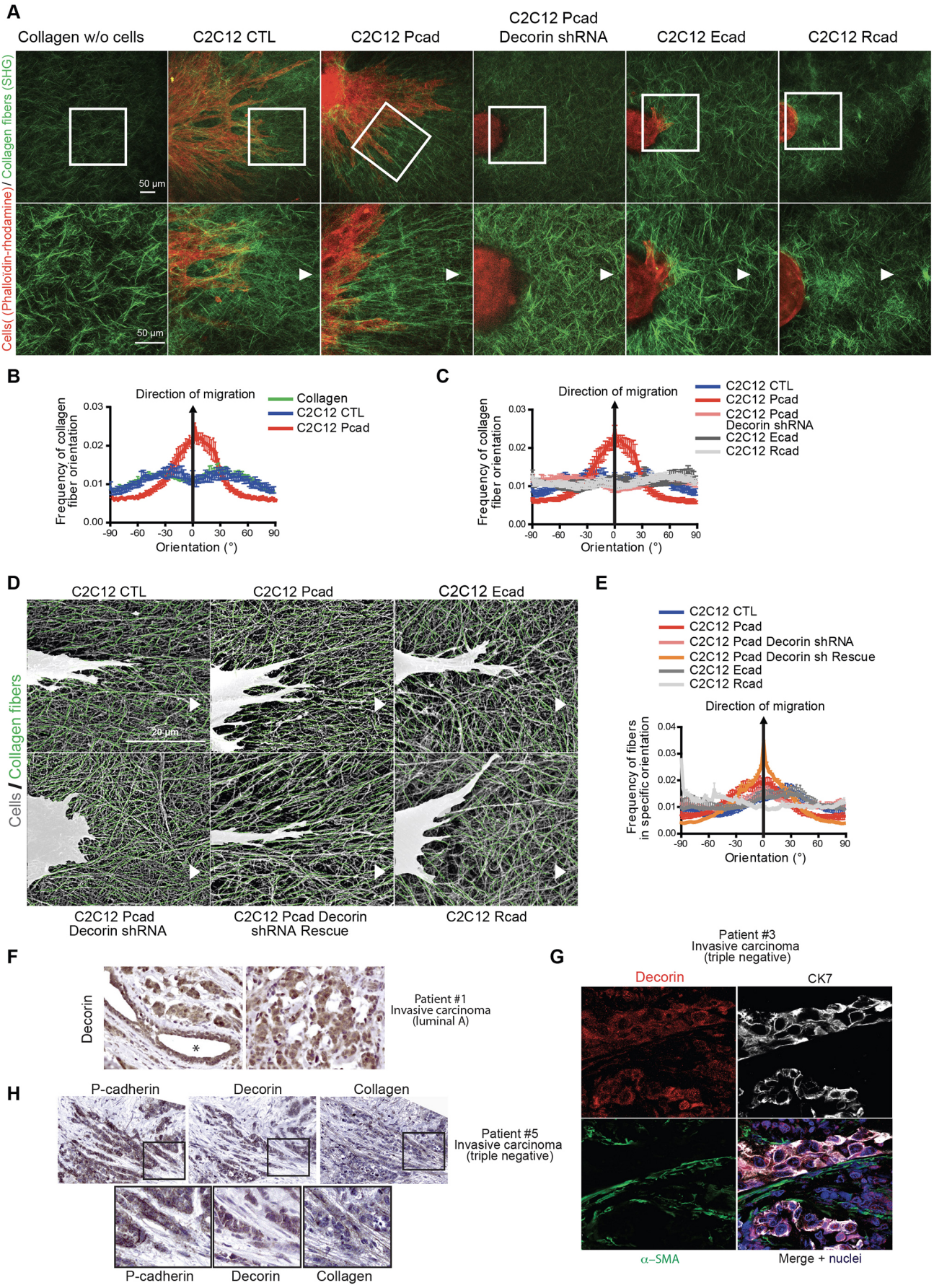

Fig. 4. See next page for legend.

Journal of Cell Science (2019) 132, jcs233189. doi:10.1242/jcs.233189

Fig. 4. Decorin is required for P-cadherin-mediated collagen fiber orientation in the migration direction. (A) Representative SHG images of fibrillar type I collagen (2 mg/ml) polymerized at 37°C (green) and of a spheroid stained with Rhodamine–phalloidin (F-actin probe; red). Bottom panels show enlargements of the boxed regions. All panels are representative of three independent experiments. Arrowheads indicate the cell migration direction. Scale bars: 50 µm. (B,C) Collagen fiber directionality analysis of the spheroid cells shown in A; 0° is the migration direction angle. Areas analyzed: *n*=26 for C2C12 CTL, *n*=25 for C2C12 Pcad, *n*=25 for C2C12 Pcad Decorin shRNA, *n*=10 for C2C12 Ecad and *n*=9 for C2C12 Rcad from three independent experiments. (D) Representative SEM images of the indicated cell lines migrating on a collagen matrix (2 mg/ml) at 6 h after PDMS membrane removal. They are an example of the analysis performed with the CurveAlign software to identify all collagen fibers (green) present in the SEM images. All panels are representative of least three independent experiments. White arrowheads indicate the migration direction. Scale bar: 20 µm. (E) Analysis of collagen fiber directionality in the cell lines shown in D; 0° is the direction of migration angle. Number of collagen fibers analyzed: *n*=12,789 for C2C12 CTL, *n*=12,520 for C2C12 Pcad, *n*=11,762 for C2C12 Pcad Decorin shRNA, *n*=13,155 for C2C12 Pcad Decorin shRNA rescue, *n*=13,885 for C2C12 Ecad and *n*=12,161 for C2C12 Rcad cells from six independent experiments. (F) Immunohistochemistry analysis of decorin in breast tumor tissue sections. Asterisk shows a normal acinus. (G) Immunofluorescence analysis of cytokeratin-7 (CK7), α-smooth muscle actin (α-SMA) and decorin in invasive breast tumor tissue sections. Nuclei were stained with Hoechst 33342. (H) Immunohistochemistry analysis of serial breast tumor tissue sections to detect P-cadherin, decorin and collagen I.

associated with better prognosis. Decorin expression has also been associated with poor prognosis in mammary and ovarian tumors (Cawthorn et al., 2012; Newton et al., 2006) and shown to have the highest expression in the most invasive breast tumor cells (Denisov et al., 2017). It is also correlated with the formation of a collagenous-rich stroma associated with microdensity, and is detected in the tumor stroma of non-palpable breast carcinoma specimens with high microdensity and micro-calcifications (Skandalis et al., 2011). Our transcriptomic analysis showed that *Dcn* is strongly upregulated upon P-cadherin expression. We confirmed that only P-cadherin (and not E- or R-cadherin) promotes decorin expression and secretion. This P-cadherin–decorin link is also observed in the MCF10A mammary cell line (Fig. S4A–C) and in discrete groups of invasive breast tumor cells (Fig. S4D) and is also supported by the observation that disease-free survival is poor in patients with $HR^{+}/ERBB2^{-}$ and $HR^{-}/ERBB2^{+}$ breast tumors with specific *CDH3*:*DCN* ratios. Moreover, by analyzing transcriptomic and proteomic data, we identified and validated interesting candidate signaling pathways activated in P-cadherin-expressing cells (i.e. the ERK, p38 and JNK MAPK signaling pathways, and the NFκB pathway; Fig. S6). Their inhibition led to a strong decrease of P-cadherin-induced persistence of migration and of *Dcn* mRNA expression in P-cadherin expressing cells (Fig. S6). *Dcn* silencing inhibited P-cadherin-induced collagen alignment and DCCM, polarization of the front protrusion and of FAs, as well as β1 integrin activation and traction force generation (Fig. 6). In clinical mammary invasive carcinoma samples, we observed aligned collagen fibers at invasion sites that were adjacent to P-cadherin- and decorin-expressing cells. This suggests that collagen fiber alignment could contribute to P-cadherin/decorin-positive cancer cell dissemination. It has been often reported that cells in the tumor microenvironment, such as cancer-associated fibroblasts, contribute to ECM molecule secretion and ECM fiber alignment (Erdogan et al., 2017). In the invasive mammary tumor samples we analyzed, decorin was expressed by tumor cells and, to a lesser extent, by cells in the tumor microenvironment (Table S6). Decorin binds not only to collagen I, but also to collagens II–VI, XII and XIV and other proteins present in the ECM, such as growth factors (Gubbiotti et al., 2016). Therefore, besides promoting collagen fiber alignment, decorin could also sequester these growth factors along the fibers to limit ligand binding in the direction of migration or to contribute to integrin stabilization for efficient migration.

During DCCM, activation of the CDC42-mediated polarity pathway is crucial for the polarization of cells, trajectories, membrane protrusions and FAs in the migration direction (Cau and Hall, 2005; Osmani et al., 2006; Plutoni et al., 2016). FA polarization in the migration direction allows force-vector orientation, resulting in higher Tx:Ty ratios and efficient DCCM. β-Pix, a guanine nucleotide exchange factor for CDC42, is involved in P-cadherin-mediated DCCM (Plutoni et al., 2016), and is activated only during migration on collagen following threonine dephosphorylation (Kutys and Yamada, 2014). We demonstrated that decorin-mediated collagen fiber remodeling is important for the activation of the β-Pix/CDC42 axis, and is required for the regulation of the polarity axis and force anisotropy that drive P-cadherin-mediated DCCM. As CDC42 activation in P-cadherin-expressing cells is integrin dependent, and β1 integrin is specifically activated by P-cadherin in a decorin-dependent manner, one could hypothesize that collagen fiber alignment is an outside-in signal for β1 integrin activation. Through this mechanism, collagen fiber alignment increases traction forces that could participate in a feedback loop to regulate collagen fiber alignment in the direction of migration.

In conclusion, our data demonstrate that collagen fiber alignment mediated by P-cadherin-induced decorin directly controls DCCM driven by the orientation and directionality of collagen fibers to promote contact guidance. This is important because *in vivo* data indicate that, in breast cancer, aligned collagen fibers in the tumor microenvironment are associated with poor prognosis. At the molecular level, collagen fiber alignment allows β1 integrin and β-Pix/CDC42 axis activation, leading to traction force generation and anisotropy that promote DCCM.

Our data suggest that decorin promotes cell migration and invasion through its role on collagen fiber alignment. This implies that anti-tumor strategies that increase decorin expression should be carefully evaluated before their transfer to the clinic.

MATERIALS AND METHODS

Cell lines

All cell lines were authenticated and tested for contamination. C2C12 mouse myoblasts (American Type Culture Collection, ATCC CRL-1772) cell lines expressing the LZRS empty vector (C2C12 CTL), P-cadherin (C2C12 Pcad), E-cadherin (C2C12 Ecad) or R-cadherin (C2C12 Rcad) were grown in DMEM supplemented with 10% fetal calf serum as described in Plutoni et al. (2016) and Thuault et al. (2013). C2C12 CTL, C2C12 Pcad, C2C12 Ecad, and C2C12 Rcad cells that stably express *Dcn* shRNAs were produced using the retroviral vector pSIREN-RetroQ. The pSIREN-RetroQ vector that targets the firefly luciferase (Luci shRNA) was used as control. Exponentially growing C2C12 myoblasts (5×10^{5} cells per 60-mm dish) were infected with 5 ml viral supernatant. Stably transfected cells were selected with 1 mg/ml G418 or 1 mg/ml puromycin (shRNAs), and different clones were isolated by limiting dilution. For rescue experiments, C2C12 Pcad Dcn shRNA cells were infected with the retroviral vector pBABE-Hygro-hDecorin 'shRNAresist' (human decorin; NCBI Reference Sequence accession no. NM_001920.4) and different clones were isolated by limiting dilution after selection with hygromycin (200 µg/ml).

shRNA constructs

shRNA constructs were generated using the retroviral vector pSIREN-RetroQ according to the manufacturer's protocol (BD Biosciences, San Diego, CA).

Journal of Cell Science (2019) 132, jcs233189. doi:10.1242/jcs.233189

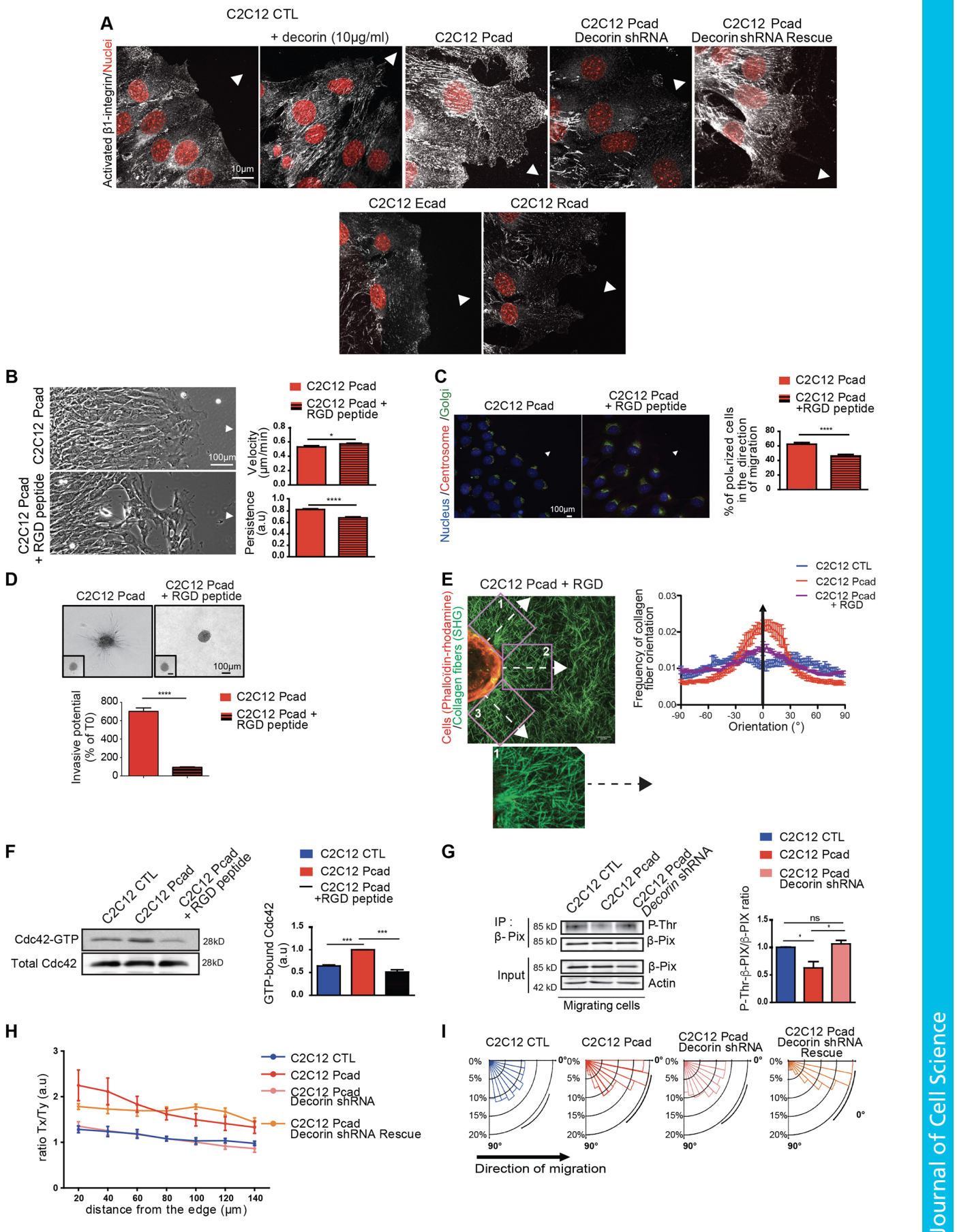

Fig. 5. See next page for legend.

Journal of Cell Science (2019) 132, jcs233189. doi:10.1242/jcs.233189

Fig. 5. Decorin is required for P-cadherin-mediated β1 integrin and CDC42 activation. (A) Immunofluorescence analysis of activated β1 integrin (9EG7 antibody) in the indicated C2C12 cell lines after 6 h of migration. Nuclei were stained with Hoechst 33342 (red). Scale bar: 10 µm. (B) Phase-contrast images of migrating C2C12 Pcad cells incubated or not with the RGD peptide (100 µM; to inhibit β1 integrin) at 10 h after barrier removal. The diagrams show the mean velocity (µm/min) and persistence (arbitrary units, a.u.) measured between 4 and 24 h after barrier removal. *n*=76 C2C12 Pcad cells, *n*=93 C2C12 Pcad cells+RGD peptide. Scale bar: 100 µm. (C) Migrating cells in the migration front were stained with Hoechst 33342 (nuclei; blue), anti-pericentrin antibody (centrosomes; red) and Alexa Fluor 488 lectin conjugates (Golgi; green) at 6 h after insert removal. The histogram shows the percentage of migrating cells in which centrosome, Golgi and nucleus were similarly aligned and oriented in the direction of migration (*n*=89 C2C12 Pcad cells, *n*=163 C2C12 Pcad cells+RGD peptide) from four independent experiments. Scale bar: 100 µm. White arrowheads in A–C represent the direction of migration. (D) Phase-contrast images of representative spheroids formed using C2C12 Pcad cells embedded in type I collagen containing 100 µM of RGD peptide for 72 h. Insets show spheroids at day 0 just after embedding. *n*=20 for each condition. Scale bar: 100 µm. Histograms show the invasive potential at 72 h of invasion. (E) Representative SHG images of fibrillar collagen (green) and of one C2C12 Pcad spheroid embedded in type I collagen containing 100 µM of RGD peptide for 72 h and stained with Rhodamine–phalloidin (F-actin probe; red). The arrows indicate the reference axis used as the cell migration direction. Squares are examples of three analyzed regions. A representative directionality histogram generated by the directionality ImageJ plug-in the indicated conditions is shown on the right. Scale bar: 20 µm. The histogram shows the collagen fiber directionality analysis in the indicated conditions. 0° is the reference angle (i.e. perpendicular to the spheroid, dashed line in the figure). Areas analyzed: *n*=26 for C2C12 CTL, *n*=25 for C2C12 Pcad and *n*=31 for C2C12 Pcad+RGD from three independent experiments. (F) The level of GTP-bound CDC42 was measured by using GST fused to the CRIB domain of PAK (GST-CRIB) in lysates from C2C12 Pcad cells incubated or not with the RGD peptide at 6 h after wounding. The histogram shows the quantification of GTP-bound CDC42 normalized to the amount of total CDC42. (G) Western blot analysis of β-Pix immunoprecipitated (IP) from migrating C2C12 CTL, Pcad and Pcad Dcn shRNA cells using anti-phosphorylated threonine, -β-Pix and -actin antibodies. The histogram represents the ratio of β-Pix threonine phosphorylation relative to total β-Pix. (H) Traction forces in the *x* direction (Tx; i.e. parallel to the migration axis), and in the *y* direction (Ty; i.e. perpendicular to the migration axis) were measured every 20 µm from the multicellular leading row towards the center of the layer from 4 to 10 h after PDMS membrane removal. The histogram shows the Tx:Ty ratio relative to the distance from the edge. (I) Rose plot showing the overall orientation of traction forces between 0 and 40 µm from the edge. The area of each bin represents the number of traction forces in that direction. 0° is the direction of migration angle (black arrow). The standard deviation is indicated on each rose plot, and all panels represent the results of four independent experiments. Data represent the means±s.e.m. of four independent experiments. **P*<0.05; ***P*<0.01; ****P*<0.001; *****P*<0.0001; ns, not significant [two-tailed Mann–Whitney test (F,G), two-tailed Student's *t*-test (B–D)].

To suppress endogenous *Dcn* expression, the annealed double-strand oligonucleotides 5′GATCCG**GCATCTCAGACACCAACATAA**TTCAAGAG-A**TTATGTTGGTGTCTGAGATGC** CTTTTTTACGCGTG 3′ (forward) and 5′-AATTCACGCGTAAAAAAG **GCATCTCAGACACCAACATA-A**TCTCTTGAA**TTATGTTGGTGTCTGAGATGC**CG-3′ (reverse) (*Dcn* shRNA2) and 5′-GATCCG**GCCGAACTCTAGCAATGTATT**TTCAAG-AGA**AATACATTGCTAGAGTTCGGC**CTTTTTTACGCGTG-3′ (forward) and 5′-AATTCACGCGTAAAAAAG **GCCGAACTCTAGCAATG-TATT**TCTCTTGAA**AATACATTGCTAGAGTTCGGC**CG-3′ (reverse) (*Dcn* shRNA3) were inserted in the RNAi-Ready pSIREN-RetroQ vector (Clontech, Mountain View, CA). Bold letters correspond to positions 902–923 and 1725–1746 of the mouse decorin cDNA sequence, NM_001190451.2). The control luciferase shRNA was made by inserting the oligonucleotide 5′-GATCCG**TGCGTTGCTAGTACCAAC**TTCAAGAGA**GTTGGT-ACTAGCAACGCA**CTTTTTTGCTAGCGAATTC-3′. Bold letters correspond to oligonucleotide 1310–1328 of the *Photinus pyralis* (firefly) luciferase sequence (GenBank accession no. M15077.1).

Transcriptomic analysis

Affymetrix microarrays were processed at the Institute in Regenerative Medicine and Biotherapy Microarray Core Facility, CHU-INSERM-UM Montpellier (http://www.chu-montpellier.fr/fr/irmb/). Briefly, biotinylated cRNAs from control C2C12 CTL cells and C2C12 Pcad cells (clones #2 and #9; Thuault et al., 2013) were prepared according to the Affymetrix GeneAtlas IVT Express protocol from 100 ng of total RNA (GeneAtlas 3'IVT ExpressTechnical Manual, 2010, P/N702833 Rev4 Affymetrix). After fragmentation, 10 µg of cRNA were hybridized at 45°C on the Affymetrix® MG-430PM Array for 16 h. StripChips were washed and stained on the fluidic station of the Affymetrix GeneAtlas system with the HWS kit. GeneChips were scanned using the Affymetrix GeneAtlas scanner and data were generated with the Affymetrix Expression Console v 1.2.1 and the GCRMA algorithm. Microarray data has been deposited in ArrayExpress under accession no. E-MTAB-8479.

Gene functional classification – GO term enrichment analysis

The PANTHER (protein annotation through evolutionary relationship, version 14.0) classification system (http://www.pantherdb.org/) was used to perform a Gene Ontology (GO) enrichment analysis. Enriched terms were considered statistically significant when p_{adj} was <0.05, and a minimum of five genes were grouped for each significant term. GO terms were categorized in three major functional groups: biological process, molecular function and cellular component.

The Gene Ontology enRIchment anaLysis and visuaLizAtion tool (GORILLA) classification system (http://cbl-gorilla.cs.technion.ac.il/) was used to perform a GO term enrichment visualization. GO terms were categorized in three major functional groups: biological process, molecular function and cellular component. The relationship between GO terms is described by a directed acyclic graph (DAG).

RNA isolation and RT-PCR analysis

Total RNA was extracted from the different cell lines using the RNeasy Mini Kit (Qiagen) according to the manufacturer's instructions. Then, RNA was reverse transcribed to cDNA using SuperScript II Reverse Transcriptase (Thermo Fisher Scientific) and real-time PCR was performed using a LightCycler 480 instrument (Roche) with the SYBR Green PCR Master Mix (Roche). The primer sequences were as follows: *Dcn*, forward, 5′-TTCCTACTCGGCTGTGAGTC-3′ and reverse, 5′-AAGTTGAATGG-CAGAACGC-3′; and, *Rpl32*, forward, 5′-TTAAGCGAAACTGGCGGA-AAC-3′ and reverse, 5′-TTGTTGCTCCCATAACCGATG-3′.

Antibodies and reagents

Mouse antibodies were against: P-cadherin (1:1000, 32-40000, Invitrogen), CDC42 (1:300, 610928, BD Transduction Laboratories), β-Pix (1:1000, 611648, BD Transduction Laboratories), paxillin (1:500, 610051, BD Transduction Laboratories) and β-actin (1:1000, 611648, BD Transduction Laboratories). A rabbit monoclonal antibody was used against phosphorylated threonine residues (1:100, 8954, Cell Signaling Technology). Rabbit polyclonal antibodies were used against pericentrin (1:150, PRB-432C, Eurogentec) and decorin (1:1000 for western blotting and 1:100 for immunofluorescence, LF-113 provided by Larry Fisher, NIH, Bethesda, MD). A rabbit polyclonal antibody against the SH3 domain of β-Pix (aa 1–65) was provided by Nathalie Morin (CRBM, 34293 Montpellier, France). F-actin was detected with Rhodamine–phalloidin (1:10,000, P1951, Sigma-Aldrich); nuclei were stained with Hoechst 33342 (1:2000, B2261, Sigma-Aldrich), The Golgi was detected using Alexa Fluor 488–lectin conjugates from *Helix pomatia* (L11271, Molecular Probes), activated β1 integrin was detected with the rat anti-mouse CD29 (1:100, 553715, Clone 9EG7, BD Transduction Laboratories) and β1 integrin with the clone MB1.2 antibody (1:100, mab1997, Millipore). Primary antibodies were detected with Alexa Fluor 488- or 546-conjugated goat anti-mouse or anti-rabbit IgG antibodies (Molecular Probes). The β1 integrin inhibitor (RGD peptide: N-CGPKGDRGDAGPKGA-C from GENECUST) was used at 100 µM and decorin (from bovine articular cartilage D8428 Sigma-Aldrich) at 10 µg/ml. After insert removal, cells were incubated with fresh medium containing the compounds and renewed every 6 h.

Journal of Cell Science (2019) 132, jcs233189. doi:10.1242/jcs.233189

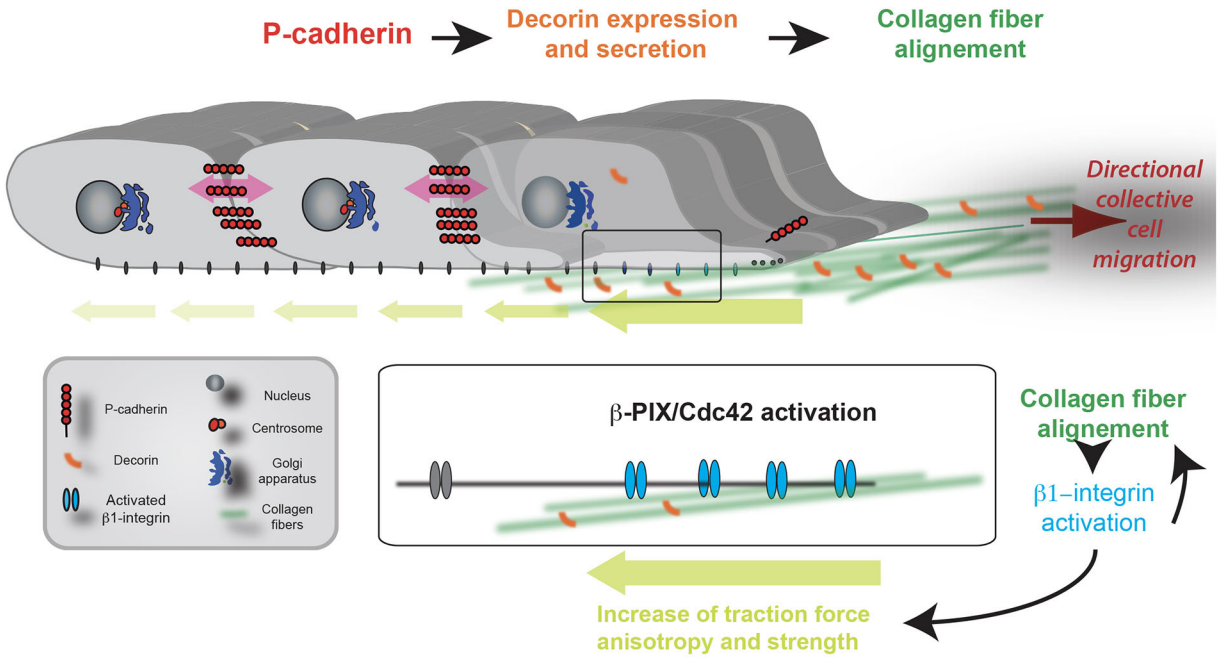

Fig. 6. Model for the role of P-cadherin-mediated decorin expression in DCCM. P-cadherin expression and homotypic interactions promote DCCM through decorin expression and secretion that allow collagen fiber alignment in the migration direction, promoting contact guidance. Decorin-mediated collagen fiber alignment induces activation of β1 integrin, which in turn potentiates collagen fiber reorganization and alignment in the direction of migration, and of the β-Pix/CDC42 axis, a key signaling pathway that controls polarization of cells, cell trajectories, membrane protrusions and FAs in the migration direction. FA polarization in the migration direction promotes force-vector orientation, resulting in a higher Tx:Ty ratio, and thus efficient DCCM.

RT-qPCR analysis of breast tumor samples

Dcn and P-cadherin mRNA levels in tumor samples from a cohort of patients with breast cancer were analyzed as described previously (Rosse et al., 2014).

Patients and specimens

Patients (n=15) with breast carcinoma were treated at the Cancer Research Institute, Tomsk NRMC (Tomsk, Russia) (Tables S6 and S7). The histological type was defined according to the World Health Organization recommendations (Lakhani et al., 2012). Tumor grade was determined using the Bloom and Richardson grading system (Bloom and Richardson, 1957). The expression of estrogen receptor (ER) and progesterone receptor (PR) was scored using the HSCORE method (Kinsel et al., 1989). HER2 expression was analyzed by immunohistochemistry and calculated on a scale 0–3+, according to the ASCO/CAP guidelines (Wolff et al., 2007). Ki-67 expression was calculated as the percentage of Ki-67-positive cells relative to all cells. Molecular subtypes were categorized on the basis of the primary tumor ER, PR, HER2, and Ki-67 status, according to the St Gallen recommendations (Wolff et al., 2007): luminal A (ER^+ and/or PR^+, $HER2^-$, and Ki-67<20%), luminal B (ER^+ and/or PR^+, $HER2^{+/-}$, and Ki-67≥20%), $HER2^+$ (ER^- and PR^-, $HER2^+$), and triple-negative (ER^-, PR^-, $HER2^-$).

Frozen and formalin-fixed paraffin-embedded (FFPE) tumor tissue specimens obtained during surgery were used for immunohistochemical and immunofluorescence analyses.

The study procedures were in accordance with the Helsinki Declaration (1964, amended in 1975 and 1983). This study was approved by the institutional review board; all patients signed an informed consent for voluntary participation.

Immunohistochemical staining

Immunohistochemical staining was used for the standard scorings (ER, PR, HER2 and Ki-67) and to assess P-cadherin, decorin, type I collagen and CK7 expression using primary mouse antibodies against ER (IR657, clone 1D5, ready-to-use, Dako, Denmark), PR (IR068, clone PgR636, ready-to-use, Dako, Denmark), Ki-67 (M306, clone SP6, ready-to-use, Spring Bioscience), and primary rabbit antibodies against HER2 (A0485, 1:800, Dako, Denmark), P-cadherin (1:50, in-house rabbit antibody; Thuault et al., 2013), decorin (1:100, LF113, from Larry Fisher) and type I collagen (1:100, 20111, Novotec). Immunohistochemical staining was performed as previously described (Zavyalova et al., 2013).

Immunofluorescence staining

FFPE tumor sections (7 µm thick) were deparaffinized, rehydrated and processed for heat-induced epitope retrieval with EDTA buffer (pH 8.0) using PT Link (Dako, Denmark), and blocked with 3% bovine serum albumin (BSA; Amresco) in PBS. Sections were incubated with primary antibodies against CK7 (clone N-20, 1:50, Santa Cruz Biotechnology), α-SMA (clone 1A4, 1:500, Dako, Denmark), P-cadherin (1:50, in-house rabbit antibody) and decorin (LF113, Larry Fischer). The secondary antibodies were: donkey anti-mouse-IgG conjugated to Alexa Fluor 488 (Abcam), donkey anti-rabbit-IgG conjugated to Cy3 (Abcam), and donkey anti-goat-IgG conjugated to Alexa Fluor 647 (Abcam). Sections were mounted with Vectashield mounting medium (Vector Laboratories, USA) containing DAPI (for nuclear staining). Samples were analyzed with a LSM 780 NLO confocal microscope (Carl Zeiss, Germany).

Alternatively, expression of P-cadherin (1:50, in-house rabbit antibody), decorin (1:100, LF113, from Larry Fisher), collagen I (1:100, 20111, Novotec) and cytokeratin 7 (CK7, clone N-20, 1:50, Santa Cruz Biotechnology) was assessed using the BondRXm immunostainer (Leica, Germany) and the Opal 7-Color Automation immunohistochemistry Kit (PerkinElmer). Samples were analyzed using the Vectra 3.0 Automated Quantitative Pathology Imaging System (PerkinElmer).

Gel electrophoresis and immunoblotting

Protein extracts (20 to 60 µg) prepared as previously described (Thuault et al., 2013) were resolved on 10% or 15% polyacrylamide gels and transferred to Immobilon-P membranes (Millipore) that were incubated with the indicated antibodies, as described previously (Thuault et al., 2013). The Odyssey Infrared Imaging System (LI-COR Biosciences) was used for protein detection and quantification. Immunoblots were quantified with Odyssey V3.0 and ImageJ.

To remove O-linked GAG chains from decorin, cell culture medium or whole-cell lysates was digested with chondroitinase ABC (Amsbio, 0.1 unit/100 mg of protein) at 37°C for 24 h, and then supernatants were concentrated by ammonium sulfate precipitation (0.4 g/ml overnight).

Immunoprecipitation of β-Pix and GTPase CDC42 activity assay

For global GTPase activity measurements and β-Pix immunoprecipitation, DCCM was induced in confluent cell monolayers using a device designed to perform multiple calibrated and reproducible injuries with a spiral scarificator (Plutoni et al., 2016). After 6 h of migration, cells were processed to measure CDC42 activity as described previously (Plutoni et al., 2016); 1 mg of the supernatant of a cell lysate obtained in buffer (10 mM PIPES pH 7, 100 mM NaCl, 300 mM sucrose, 3 mM MgCl2, 0.5% IGEPAL CA-640, 1 mM EDTA, 1 mM Na3 VO4, protease inhibitor cocktail) was used for immunoprecipitation. The polyclonal anti-β-PIX antibody was incubated with protein G (Dynabeads; Invitrogen) at room temperature for 30 min. After washing, 1 mg protein extract was added at room temperature for 3 h.

Immunofluorescence of 2D migrating cells

Cells were plated in Ibidi culture inserts on 12-mm-diameter cover-slips until they reached the desired density level. At 5–10 h after insert removal, cells were fixed in 3.2% paraformaldehyde (PFA) in PBS for 15 min, followed by 2 min permeabilization with 0.1% Triton X-100 (in PBS) and saturation with 2% BSA (in PBS). Cells were incubated with primary and secondary antibodies in PBS containing 2% BSA. After washing with PBS with 2% BSA, primary antibodies were detected with Alexa Fluor 488-conjugated goat anti-rabbit-IgG or -mouse-IgG in PBS with 1% BSA. Images were taken using a confocal SP5-SMD (Leica) with 40×/1.3 NA or 63×/1.4 NA oil HCX PL APO CS objectives (Leica) and captured with a hybrid detector (Leica HyD) controlled using the C software. Images were processed using Adobe Photoshop and assembled using Adobe Illustrator.

3D invasion assay

Spheroids were prepared as described previously (Thuault et al., 2013) and embedded in neutralized 3D collagen (2 ml/ml, rat-tail Corning) matrix according to the manufacturer's instructions. The RDG (100 µM) was added to the collagen. Spheroid invasion was monitored for 72 h using an Olympus IX-83 microscope equipped with a motorized stage, and heated and CO_2-regulated incubator. Phase-contrast images were taken every hour, using a 10×/0.3 NA RC objective and captured with a sCMOS Zyla 4.2.1 camera controlled by the Metamorph software. The invaded area occupied by the cells was measured using ImageJ (http://dev.mri.cnrs.fr/projects/imagej-macros/wiki/Phase_Contrast_Cell_Analysis_Tool_%28Trainable_WEKA_Segmentation%29). Detached cells (characterized by loss of cell–cell adhesion) were counted at 72 h of invasion. Data are the mean±standard error of the mean (s.e.m.) of at least four independent experiments in which at least five spheroids were embedded per experimental condition.

Imaging of 3D collagen fiber organization and quantification of collagen fiber orientation

Cell spheroids embedded in type I collagen matrix for 72 h were fixed in 4% PFA in PBS at 37°C for 2 h. Samples were blocked and permeabilized in a 1% BSA and 0.1% Triton X-100 PBS solution for 2 h, stained with Rhodamine–phalloidin in 1% BSA in PBS at 4°C overnight. For observation, each spheroid-containing collagen sample was mounted in a PDMS tube between a slide and a coverslip. Samples were observed using a multiphoton Zeiss LSM 7MP Optical Parametric Oscillator microscope using a 20×/1.0 NA Plan Apochromat water immersion objective and PMT NDD detectors, controlled by the Zeiss Zen software. The collagen network was imaged by SHG combined with imaging of Rhodamine–phalloidin-labeled cells using the 1079 nm line. Z-stacks with a spacing of 1 µm were collected to obtain an accurate visualization of the collagen fibers. Images of collagen fibers in contact with the spheroid were analyzed using ImageJ (directionality plug-in) to measure the 2D-projected angles of all fibers and to obtain the alignment coefficient (Grossman et al., 2016). The migration axis is the perpendicular to the spheroid.

2D collagen fiber organization imaging and quantification of collagen fiber orientation

Polyacrylamide gels were prepared as previously described to support coating with neutralized type I collagen (2 mg/ml, Corning) (Plutoni et al., 2016). After polymerization at 37°C for 1 h, a PDMS membrane with a rectangular opening was deposited on top of the collagen-coated polyacrylamide gel. Then, 20,000 cells were seeded within the rectangle defined by the PDMS membrane opening. Cells were left to adhere and proliferate for a few hours. Then, the PDMS membrane was carefully removed, to allow cells to migrate towards the available substrate. After 12 h of migration, cells were fixed with 2.5% glutaraldehyde and dehydrated with ethanol and then with hexamethyldisilazane (HMDS). Samples were shaded with sprayed gold and observed using a scanning electron microscope (Hitachi S4000). For quantification of collagen fiber orientation, the ImageJ directionality plugin was used (Grossman et al., 2016).

Time-lapse imaging and measurements of cell velocity, persistence and directionality, and particle velocimetry analysis

Cells were plated in Ibidi Culture-Inserts (BioValley; 20,000 cells per chamber) until they reached the desired density level. Then, inserts were removed to allow cells to migrate into the cell-free areas. Cells were imaged using an Axiovert inverted microscope (Carl Zeiss) equipped with a motorized stage, and heated and CO_2 regulated incubator. Phase-contrast images were taken every 5 min overnight using a 10×/0.3 NA PH1 DIC1 objective and captured with a CCD MicroMax 1300 Y/HS camera (Roper Scientific) controlled by the MetaMorph 7.0 software.

Manual cell tracking and *x*/*y* cell position recording (of each cell at each time point) were performed using MetaMorph software. The mean speed, persistence and directionality of individual cells were calculated and illustrated using the Ibidi Chemotaxis tool (https://ibidi.com/chemotaxis-analysis/171-chemotaxis-and-migration-tool.html). Angles were plotted using the Rose.net software. The velocity field in monolayers was mapped by particle imaging velocimetry (PIV) analysis as previously described (Plutoni et al., 2016).

Cell polarity measurement

At 5–10 h after insert removal, cells were fixed, and nuclei, centrosomes and the Golgi were stained. Cells in the first four rows of the 2D migrating cells were analyzed. Measurements of cell polarity toward a global monolayer direction (centrosomes located in front of the nucleus and behind the Golgi apparatus within the quadrant facing the wound) were scored as correctly oriented (Osmani et al., 2006).

FA and membrane protrusion orientation

Confocal images of paxillin or F-actin staining were taken 6 h after insert removal. FA orientation, membrane protrusion size and orientation were measured using ImageJ, and angle values were plotted using the Rose.Net software. Each orientation was determined using the monolayer migration direction as reference axis.

Cell monolayer patterning, time-lapse microscopy and traction-force microscopy

Briefly, polyacrylamide gels with a Young's modulus of 12 kPa were prepared as previously described (Plutoni et al., 2016). After polymerization, gels were incubated with 0.1 mg/ml collagen I overnight. Then, to pattern the cells on top of the polyacrylamide gels, a PDMS membrane with a rectangular opening was deposited on top of the polyacrylamide gel and cells were seeded and left to adhere and proliferate for a few hours. Then, the PDMS membrane was carefully removed and cells could migrate toward the available substrate. Time-lapse imaging was performed using an automated inverted microscope (Nikon Eclipse Ti, 10× objective lens) equipped with thermal, CO_2 and humidity controls operated by the MetaMorph software (Universal Imaging) software. Recording started ∼30 min after removal of the PDMS membrane and lasted for 15 h. Images were obtained every 3 min over a period of 1 to 15 h. As cells migrated, they exerted traction forces on the substrate, resulting in polyacrylamide gel deformations that could be observed by imaging the

displacements of fluorescent beads embedded in the gel. Bead displacement between any experimental time point and a reference image obtained after cell trypsinization was computed using an in-house PIV algorithm (available upon request). Based on these displacements, traction forces were computed using Fourier transform traction microscopy with finite gel thickness, as described in Trepat et al. (2009).

Monolayer stress microscopy

To compute maps of the mechanical inter- and intra-cellular tension within monolayer sheets, monolayer stress microscopy was used as previously described (Tambe et al., 2011). According to Newton's law, traction forces applied at the cell–gel interface must be balanced by intra- and inter-cellular forces (Serra-Picamal et al., 2015; Tambe et al., 2011, 2013). The alignment angle between the major axis of the principal stress ellipse and the direction of the cellular motion was measured as previously described (Serra-Picamal et al., 2015).

Statistical analysis

To assess significant differences between experimental conditions, Student's *t*-tests (experiments with $n>30$) and non-parametric Mann–Whitney *U*-tests (experiments with $n<30$) were used. At least three independent experiments were performed.

Metastasis-free survival (MFS) was determined as the interval between initial diagnosis and detection of the first metastasis. Survival distributions were estimated by the Kaplan–Meier method and the significance of differences between survival rates were ascertained with the log-rank test.

Acknowledgements

We thank Virginie Georget, Hassan Boukhaddaoui, Sylvain de Rossi, Simon Lachambre, Chantal Cazevieille, Alicia Cabalerro-Medigo and Vicky Dialou from the Montpellier Imaging Facility (http://www.mri.cnrs.fr/); the Institute in Regenerative Medicine and Biotherapy Microarray Core Facility, CHU-INSERM-UM Montpellier (http://www.chu-montpellier.fr/fr/irmb/) for the transcriptomic arrays and analysis. Mass spectrometry experiments were carried out at of the Functional Proteomics Platform Facility of Montpellier. We acknowledge Larry W. Fisher for the anti-decorin antibody, and Damien Planchon, Mallory Genest, Eva Faurobert, Corinne Albigès-Rizo, Matthew Kutys, Didier Fesquet and Florence Ruggiero for helpful discussions. The Montpellier Imaging Facility is supported by the Agence Nationale de la Recherche (ANR-10-INBS-04, 'Investments for the future').

Competing interests

The authors declare no competing or financial interests.

Author contributions

Conceptualization: M.L.B.-R., L.A., L.O., L.A.T., M.S.; Methodology: M.L.B.-R., E.B., L.O., F.C., L.A.T., S.V., C.P., M.S.; Validation: L.A., E.B., S.V.; Formal analysis: M.S.; Investigation: M.L.B.-R., L.A., L.O., F.C., L.A.T., S.V., C.P.; Resources: E.V.D., I.B.; Data curation: E.B., F.C., L.A.T., S.B.; Writing - original draft: M.L.B.-R., E.B., E.V.D.; Writing - review & editing: S.B., C.G.-R.; Visualization: M.L.B.-R., I.B., C.P., C.G.-R.; Supervision: F.C., E.V.D., V.M.P., I.B., S.B., C.G.-R.; Project administration: C.G.-R.; Funding acquisition: E.V.D., V.M.P., C.G.-R.

Funding

This work was supported by the Ligue Contre le Cancer (LNCC) and the Fondation pour la Recherche Médicale (FRM) and the Russian Science Foundation (grant 19-75-30016). C.G.R. was supported by Institut National de la Santé et de la Recherche Médicale (INSERM) and M.L.B.-R. by the Ligue Nationale contre le Cancer (LNCC).

Data availability

Microarray data has been deposited in ArrayExpress under accession no. E-MTAB-8479.

Supplementary information

Supplementary information available online at
http://jcs.biologists.org/lookup/doi/10.1242/jcs.233189.supplemental

References

Banerjee, A. G., Bhattacharyya, I., Lydiatt, W. M. and Vishwanatha, J. K. (2003). Aberrant expression and localization of decorin in human oral dysplasia and squamous cell carcinoma. *Cancer Res.* **63**, 7769-7776.

Bazellières, E., Conte, V., Elosegui-Artola, A., Serra-Picamal, X., Bintanel-Morcillo, M., Roca-Cusachs, P., Munoz, J. J., Sales-Pardo, M., Guimera, R. and Trepat, X. (2015). Control of cell-cell forces and collective cell dynamics by the intercellular adhesome. *Nat. Cell Biol.* **17**, 409-420. doi:10.1038/ncb3135

Bloom, H. J. and Richardson, W. W. (1957). Histological grading and prognosis in breast cancer; a study of 1409 cases of which 359 have been followed for 15 years. *Br. J. Cancer* **11**, 359-377. doi:10.1038/bjc.1957.43

Bozoky, B., Savchenko, A., Guven, H., Ponten, F., Klein, G. and Szekely, L. (2014). Decreased decorin expression in the tumor microenvironment. *Cancer Med.* **3**, 485-491. doi:10.1002/cam4.231

Cau, J. and Hall, A. (2005). Cdc42 controls the polarity of the actin and microtubule cytoskeletons through two distinct signal transduction pathways. *J. Cell Sci.* **118**, 2579-2587. doi:10.1242/jcs.02385

Cawthorn, T. R., Moreno, J. C., Dharsee, M., Tran-Thanh, D., Ackloo, S., Zhu, P. H., Sardana, G., Chen, J., Kupchak, P., Jacks, L. M. et al. (2012). Proteomic analyses reveal high expression of decorin and endoplasmin (HSP90B1) are associated with breast cancer metastasis and decreased survival. *PLoS ONE* **7**, e30992. doi:10.1371/journal.pone.0030992

Chen, S. and Birk, D. E. (2013). The regulatory roles of small leucine-rich proteoglycans in extracellular matrix assembly. *FEBS J.* **280**, 2120-2137. doi:10.1111/febs.12136

Conklin, M. W., Eickhoff, J. C., Riching, K. M., Pehlke, C. A., Eliceiri, K. W., Provenzano, P. P., Friedl, A. and Keely, P. J. (2011). Aligned collagen is a prognostic signature for survival in human breast carcinoma. *Am. J. Pathol.* **178**, 1221-1232. doi:10.1016/j.ajpath.2010.11.076

Csordás, G., Santra, M., Reed, C. C., Eichstetter, I., McQuillan, D. J., Gross, D., Nugent, M. A., Hajnóczky, G. and Iozzo, R. V. (2000). Sustained down-regulation of the epidermal growth factor receptor by decorin: a mechanism for controlling tumor growth *in vivo*. *J. Biol. Chem.* **275**, 32879-32887. doi:10.1074/jbc.M005609200

Danielson, K. G., Baribault, H., Holmes, D. F., Graham, H., Kadler, K. E. and Iozzo, R. V. (1997). Targeted disruption of decorin leads to abnormal collagen fibril morphology and skin fragility. *J. Cell Biol.* **136**, 729-743. doi:10.1083/jcb.136.3.729

Denisov, E. V., Skryabin, N. A., Gerashchenko, T. S., Tashireva, L. A., Wilhelm, J., Buldakov, M. A., Sleptcov, A. A., Lebedev, I. N., Vtorushin, S. V., Zavyalova, M. V. et al. (2017). Clinically relevant morphological structures in breast cancer represent transcriptionally distinct tumor cell populations with varied degrees of epithelial-mesenchymal transition and $CD44^{+}CD24^{-}$ stemness. *Oncotarget* **8**, 61163-61180. doi:10.18632/oncotarget.18022

Dil, N. and Banerjee, A. G. (2011). A role for aberrantly expressed nuclear localized decorin in migration and invasion of dysplastic and malignant oral epithelial cells. *Head Neck Oncol.* **3**, 44. doi:10.1186/1758-3284-3-44

Dil, N. and Banerjee, A. G. (2012). Knockdown of aberrantly expressed nuclear localized decorin attenuates tumour angiogenesis related mediators in oral cancer progression model in vitro. *Head Neck Oncol.* **4**, 11. doi:10.1186/1758-3284-4-11

Doyle, A. D., Wang, F. W., Matsumoto, K. and Yamada, K. M. (2009). One-dimensional topography underlies three-dimensional fibrillar cell migration. *J. Cell Biol.* **184**, 481-490. doi:10.1083/jcb.200810041

Drifka, C. R., Loeffler, A. G., Mathewson, K., Keikhosravi, A., Eickhoff, J. C., Liu, Y., Weber, S. M., John Kao, W. and Eliceiri, K. W. (2016). Highly aligned stromal collagen is a negative prognostic factor following pancreatic ductal adenocarcinoma resection. *Oncotarget* **7**, 76197-76213. doi:10.18632/oncotarget.12772

Eden, E., Navon, R., Steinfeld, I., Lipson, D. and Yakhini, Z. (2009). GOrilla: a tool for discovery and visualization of enriched GO terms in ranked gene lists. *BMC Bioinformatics* **10**, 48. doi:10.1186/1471-2105-10-48

Egeblad, M., Rasch, M. G. and Weaver, V. M. (2010). Dynamic interplay between the collagen scaffold and tumor evolution. *Curr. Opin. Cell Biol.* **22**, 697-706. doi:10.1016/j.ceb.2010.08.015

El Behi, M., Krumeich, S., Lodillinsky, C., Kamoun, A., Tibaldi, L., Sugano, G., De Reynies, A., Chapeaublanc, E., Laplanche, A., Lebret, T. et al. (2013). An essential role for decorin in bladder cancer invasiveness: Immune system and decorin in bladder tumour progression. *EMBO Mol. Med.* **5**, 1835-1851. doi:10.1002/emmm.201302655

Erdogan, B., Ao, M., White, L. M., Means, A. L., Brewer, B. M., Yang, L., Washington, M. K., Shi, C., Franco, O. E., Weaver, A. M. et al. (2017). Cancer-associated fibroblasts promote directional cancer cell migration by aligning fibronectin. *J. Cell Biol.* **216**, 3799-3816. doi:10.1083/jcb.201704053

Fiedler, L. R., Schönherr, E., Waddington, R., Niland, S., Seidler, D. G., Aeschlimann, D. and Eble, J. A. (2008). Decorin regulates endothelial cell motility on collagen i through activation of insulin-like growth factor i receptor and modulation of 2 1 integrin activity. *J. Biol. Chem.* **283**, 17406-17415. doi:10.1074/jbc.M710025200

Friedl, P. and Gilmour, D. (2009). Collective cell migration in morphogenesis, regeneration and cancer. *Nat. Rev. Mol. Cell Biol.* **10**, 445-457. doi:10.1038/nrm2720

Friedl, P., Locker, J., Sahai, E. and Segall, J. E. (2012). Classifying collective cancer cell invasion. *Nat. Cell Biol.* **14**, 777-783. doi:10.1038/ncb2548

Gaggioli, C., Hooper, S., Hidalgo-Carcedo, C., Grosse, R., Marshall, J. F., Harrington, K. and Sahai, E. (2007). Fibroblast-led collective invasion of

carcinoma cells with differing roles for RhoGTPases in leading and following cells. *Nat. Cell Biol.* **9**, 1392-1400. doi:10.1038/ncb1658

Gjorevski, N., Piotrowski, A. S., Varner, V. D. and Nelson, C. M. (2015). Dynamic tensile forces drive collective cell migration through three-dimensional extracellular matrices. *Sci. Rep.* **5**, 11458. doi:10.1038/srep11458

Goetsch, K. P., Kallmeyer, K. and Niesler, C. U. (2011). Decorin modulates collagen I-stimulated, but not fibronectin-stimulated, migration of C2C12 myoblasts. *Matrix Biol.* **30**, 109-117. doi:10.1016/j.matbio.2010.10.009

Grossman, M., Ben-Chetrit, N., Zhuravlev, A., Afik, R., Bassat, E., Solomonov, I., Yarden, Y. and Sagi, I. (2016). Tumor cell invasion can be blocked by modulators of collagen fibril alignment that control assembly of the extracellular matrix. *Cancer Res.* **76**, 4249-4258. doi:10.1158/0008-5472.CAN-15-2813

Gubbiotti, M. A., Neill, T., Frey, H., Schaefer, L. and Iozzo, R. V. (2015). Decorin is an autophagy-inducible proteoglycan and is required for proper in vivo autophagy. *Matrix Biol.* **48**, 14-25. doi:10.1016/j.matbio.2015.09.001

Gubbiotti, M. A., Vallet, S. D., Ricard-Blum, S. and Iozzo, R. V. (2016). Decorin interacting network: a comprehensive analysis of decorin-binding partners and their versatile functions. *Matrix Biol.* **55**, 7-21. doi:10.1016/j.matbio.2016.09.009

Haeger, A., Krause, M., Wolf, K. and Friedl, P. (2014). Cell jamming: collective invasion of mesenchymal tumor cells imposed by tissue confinement. *Biochim. Biophys. Acta* **1840**, 2386-2395. doi:10.1016/j.bbagen.2014.03.020

Halbleib, J. M. and Nelson, W. J. (2006). Cadherins in development: cell adhesion, sorting, and tissue morphogenesis. *Genes Dev.* **20**, 3199-3214. doi:10.1101/gad.1486806

Iozzo, R. V. and Schaefer, L. (2015). Proteoglycan form and function: a comprehensive nomenclature of proteoglycans. *Matrix Biol. J. Int. Soc. Matrix Biol.* **42**, 11-55. doi:10.1016/j.matbio.2015.02.003

Järvinen, T. A. H. and Prince, S. (2015). Decorin: a growth factor antagonist for tumor growth inhibition. *BioMed Res. Int.* **2015**, 1-11. doi:10.1155/2015/654765

Jasaitis, A., Estevez, M., Heysch, J., Ladoux, B. and Dufour, S. (2012). E-cadherin-dependent stimulation of traction force at focal adhesions via the Src and PI3K signaling pathways. *Biophys. J.* **103**, 175-184. doi:10.1016/j.bpj.2012.06.009

Kalamajski, S. and Oldberg, A. (2010). The role of small leucine-rich proteoglycans in collagen fibrillogenesis. *Matrix Biol.* **29**, 248-253. doi:10.1016/j.matbio.2010.01.001

Kinsel, L. B., Szabo, E., Greene, G. L., Konrath, J., Leight, G. S. and McCarty, K. S. (1989). Immunocytochemical analysis of estrogen receptors as a predictor of prognosis in breast cancer patients: comparison with quantitative biochemical methods. *Cancer Res.* **49**, 1052-1056.

Kutys, M. L. and Yamada, K. M. (2014). An extracellular-matrix-specific GEF-GAP interaction regulates Rho GTPase crosstalk for 3D collagen migration. *Nat. Cell Biol.* **16**, 909-917. doi:10.1038/ncb3026

Lakhani, S. R., International Agency for Research on Cancer and **Weltgesundheitsorganisation** (ed.). (2012). WHO classification of tumours of the breast: views of a working group that convened for a consensus and editorial meeting at the International Agency for Research on Cancer (IARC), Lyon, September 1-3, 2011. 4. ed. Internat. Agency for Research on Cancer, Lyon. 240 pp.

Levental, K. R., Yu, H., Kass, L., Lakins, J. N., Egeblad, M., Erler, J. T., Fong, S. F. T., Csiszar, K., Giaccia, A., Weninger, W. et al. (2009). Matrix crosslinking forces tumor progression by enhancing integrin signaling. *Cell* **139**, 891-906. doi:10.1016/j.cell.2009.10.027

Lyons, T. R., O'Brien, J., Borges, V. F., Conklin, M. W., Keely, P. J., Eliceiri, K. W., Marusyk, A., Tan, A.-C. and Schedin, P. (2011). Postpartum mammary gland involution drives progression of ductal carcinoma in situ through collagen and COX-2. *Nat. Med.* **17**, 1109-1115. doi:10.1038/nm.2416

Maruthamuthu, V., Sabass, B., Schwarz, U. S. and Gardel, M. L. (2011). Cell-ECM traction force modulates endogenous tension at cell-cell contacts. *Proc. Natl. Acad. Sci. USA* **108**, 4708-4713. doi:10.1073/pnas.1011123108

Mertz, A. F., Che, Y., Banerjee, S., Goldstein, J. M., Rosowski, K. A., Revilla, S. F., Niessen, C. M., Marchetti, M. C., Dufresne, E. R. and Horsley, V. (2013). Cadherin-based intercellular adhesions organize epithelial cell-matrix traction forces. *Proc. Natl. Acad. Sci. USA* **110**, 842-847. doi:10.1073/pnas.1217279110

Naba, A., Clauser, K. R., Ding, H., Whittaker, C. A., Carr, S. A. and Hynes, R. O. (2016). The extracellular matrix: tools and insights for the "omics" era. *Matrix Biol.* **49**, 10-24. doi:10.1016/j.matbio.2015.06.003

Neame, P. J., Kay, C. J., McQuillan, D. J., Beales, M. P. and Hassell, J. R. (2000). Independent modulation of collagen fibrillogenesis by decorin and lumican. *Cell. Mol. Life Sci. CMLS* **57**, 859-863. doi:10.1007/s000180050048

Newton, T. R., Parsons, P. G., Lincoln, D. J., Cummings, M. C., Wyld, D. K., Webb, P. M., Green, A. C. and Boyle, G. M. (2006). Expression profiling correlates with treatment response in women with advanced serous epithelial ovarian cancer. *Int. J. Cancer* **119**, 875-883. doi:10.1002/ijc.21823

Ng, M. R., Besser, A., Danuser, G. and Brugge, J. S. (2012). Substrate stiffness regulates cadherin-dependent collective migration through myosin-II contractility. *J. Cell Biol.* **199**, 545-563. doi:10.1083/jcb.201207148

Omelchenko, T., Rabadan, M. A., Hernández-Martínez, R., Grego-Bessa, J., Anderson, K. V. and Hall, A. (2014). beta-Pix directs collective migration of anterior visceral endoderm cells in the early mouse embryo. *Genes Dev.* **28**, 2764-2777. doi:10.1101/gad.251371.114

Orgel, J. P. R. O., Eid, A., Antipova, O., Bella, J. and Scott, J. E. (2009). Decorin core protein (Decoron) shape complements collagen fibril surface structure and mediates its Binding. *PLoS ONE* **4**, e7028. doi:10.1371/journal.pone.0007028

Osmani, N., Vitale, N., Borg, J.-P. and Etienne-Manneville, S. (2006). Scrib controls Cdc42 localization and activity to promote cell polarization during astrocyte migration. *Curr. Biol.* **16**, 2395-2405. doi:10.1016/j.cub.2006.10.026

Petitjean, L., Reffay, M., Grasland-Mongrain, E., Poujade, M., Ladoux, B., Buguin, A. and Silberzan, P. (2010). Velocity fields in a collectively migrating epithelium. *Biophys. J.* **98**, 1790-1800. doi:10.1016/j.bpj.2010.01.030

Plutoni, C., Bazellieres, E., Le Borgne-Rochet, M., Comunale, F., Brugues, A., Séveno, M., Planchon, D., Thuault, S., Morin, N., Bodin, S. et al. (2016). P-cadherin promotes collective cell migration via a Cdc42-mediated increase in mechanical forces. *J. Cell Biol.* **212**, 199-217. doi:10.1083/jcb.201505105

Pogány, G. and Vogel, K. G. (1992). The interaction of decorin core protein fragments with type I collagen. *Biochem. Biophys. Res. Commun.* **189**, 165-172. doi:10.1016/0006-291X(92)91539-3

Provenzano, P. P., Inman, D. R., Eliceiri, K. W., Knittel, J. G., Yan, L., Rueden, C. T., White, J. G. and Keely, P. J. (2008). Collagen density promotes mammary tumor initiation and progression. *BMC Med.* **6**, 11. doi:10.1186/1741-7015-6-11

Riching, K. M., Cox, B. L., Salick, M. R., Pehlke, C., Riching, A. S., Ponik, S. M., Bass, B. R., Crone, W. C., Jiang, Y., Weaver, A. M. et al. (2014). 3D collagen alignment limits protrusions to enhance breast cancer cell persistence. *Biophys. J.* **107**, 2546-2558. doi:10.1016/j.bpj.2014.10.035

Rosse, C., Lodillinsky, C., Fuhrmann, L., Nourieh, M., Monteiro, P., Irondelle, M., Lagoutte, E., Vacher, S., Waharte, F., Paul-Gilloteaux, P. et al. (2014). Control of MT1-MMP transport by atypical PKC during breast-cancer progression. *Proc. Natl. Acad. Sci. USA* **111**, E1872-E1879. doi:10.1073/pnas.1400749111

Row, S., Liu, Y., Alimperti, S., Agarwal, S. K. and Andreadis, S. T. (2016). Cadherin-11 is a novel regulator of extracellular matrix synthesis and tissue mechanics. *J. Cell Sci.* **129**, 2950-2961. doi:10.1242/jcs.183772

Santra, M., Eichstetter, I. and Iozzo, R. V. (2000). An anti-oncogenic role for decorin: down-regulation of ErbB2 leads to growth suppression and cytodifferentiation of mammary carcinoma cells. *J. Biol. Chem.* **275**, 35153-35161. doi:10.1074/jbc.M006821200

Scarpa, E. and Mayor, R. (2016). Collective cell migration in development. *J. Cell Biol.* **212**, 143-155. doi:10.1083/jcb.201508047

Scott, J. E. (1988). Proteoglycan-fibrillar collagen interactions. *Biochem. J.* **252**, 313-323. doi:10.1042/bj2520313

Scott, J. E. and Orford, C. R. (1981). Dermatan sulphate-rich proteoglycan associates with rat tail-tendon collagen at the d band in the gap region. *Biochem. J.* **197**, 213-216. doi:10.1042/bj1970213

Serra-Picamal, X., Conte, V., Sunyer, R., Munoz, J. J. and Trepat, X. (2015). Mapping forces and kinematics during collective cell migration. *Methods Cell Biol.* **125**, 309-330. doi:10.1016/bs.mcb.2014.11.003

Skandalis, S. S., Labropoulou, V. T., Ravazoula, P., Likaki-Karatza, E., Dobra, K., Kalofonos, H. P., Karamanos, N. K. and Theocharis, A. D. (2011). Versican but not decorin accumulation is related to malignancy in mammographically detected high density and malignant-appearing microcalcifications in non-palpable breast carcinomas. *BMC Cancer* **11**. doi:10.1186/1471-2407-11-314

Tambe, D. T., Hardin, C. C., Angelini, T. E., Rajendran, K., Park, C. Y., Serra-Picamal, X., Zhou, E. H., Zaman, M. H., Butler, J. P., Weitz, D. A. et al. (2011). Collective cell guidance by cooperative intercellular forces. *Nat. Mater.* **10**, 469-475. doi:10.1038/nmat3025

Tambe, D. T., Croutelle, U., Trepat, X., Park, C. Y., Kim, J. H., Millet, E., Butler, J. P. and Fredberg, J. J. (2013). Monolayer stress microscopy: limitations, artifacts, and accuracy of recovered intercellular stresses. *PLoS ONE* **8**, e55172. doi:10.1371/journal.pone.0055172

Thuault, S., Hayashi, S., Lagirand-Cantaloube, J., Plutoni, C., Comunale, F., Delattre, O., Relaix, F. and Gauthier-Rouviere, C. (2013). P-cadherin is a direct PAX3-FOXO1A target involved in alveolar rhabdomyosarcoma aggressiveness. *Oncogene* **32**, 1876-1887. doi:10.1038/onc.2012.217

Trepat, X., Wasserman, M. R., Angelini, T. E., Millet, E., Weitz, D. A., Butler, J. P. and Fredberg, J. J. (2009). Physical forces during collective cell migration. *Nat. Phys.* **5**, 426-430. doi:10.1038/nphys1269

Tufvesson, E. (2003). Biglycan and decorin induce morphological and cytoskeletal changes involving signalling by the small GTPases RhoA and Rac1 resulting in lung fibroblast migration. *J. Cell Sci.* **116**, 4857-4864. doi:10.1242/jcs.00808

van Roy, F. (2014). Beyond E-cadherin: roles of other cadherin superfamily members in cancer. *Nat. Rev. Cancer* **14**, 121-134. doi:10.1038/nrc3647

Vieira, A. F. and Paredes, J. (2015). P-cadherin and the journey to cancer metastasis. *Mol. Cancer* **14**, 178. doi:10.1186/s12943-015-0448-4

Weber, I. T., Harrison, R. W. and Iozzo, R. V. (1996). Model structure of decorin and implications for collagen fibrillogenesis. *J. Biol. Chem.* **271**, 31767-31770. doi:10.1074/jbc.271.50.31767

Wolf, K., Wu, Y. I., Liu, Y., Geiger, J., Tam, E., Overall, C., Stack, M. S. and Friedl, P. (2007). Multi-step pericellular proteolysis controls the transition from individual to collective cancer cell invasion. *Nat. Cell Biol.* **9**, 893-904. doi:10.1038/ncb1616

Wolff, A. C., Hammond, M. E. H., Schwartz, J. N., Hagerty, K. L., Allred, D. C., Cote, R. J., Dowsett, M., Fitzgibbons, P. L., Hanna, W. M., Langer, A. et al. and American Society of Clinical Oncology/College of American Pathologists. (2007). American society of clinical oncology/college of american pathologists guideline recommendations for human epidermal growth factor receptor 2 testing in breast cancer. *Arch. Pathol. Lab. Med.* **131**, 18-43. doi:10.1200/JCO.2006.09.2775

Yadav, S., Puri, S. and Linstedt, A. D. (2009). A primary role for Golgi positioning in directed secretion, cell polarity, and wound healing. *Mol. Biol. Cell* **20**, 1728-1736. doi:10.1091/mbc.e08-10-1077

Zaidel-Bar, R., Ballestrem, C., Kam, Z. and Geiger, B. (2003). Early molecular events in the assembly of matrix adhesions at the leading edge of migrating cells. *J. Cell Sci.* **116**, 4605-4613. doi:10.1242/jcs.00792

Zavyalova, M. V., Denisov, E. V., Tashireva, L. A., Gerashchenko, T. S., Litviakov, N. V., Skryabin, N. A., Vtorushin, S. V., Telegina, N. S., Slonimskaya, E. M., Cherdyntseva, N. V. et al. (2013). Phenotypic drift as a cause for intratumoral morphological heterogeneity of invasive ductal breast carcinoma not otherwise specified. *BioResearch Open Access* **2**, 148-154. doi:10.1089/biores.2012.0278